AD NUMBER
AD831097
LIMITATION CHANGES
TO: **Approved for public release; distribution is unlimited.**
FROM: **Distribution authorized to U.S. Gov't. agencies and their contractors; Critical Technology; APR 1968. Other requests shall be referred to Air Force Technical Application Center, Washington, DC 20333. This document contains export-controlled technical data.**
AUTHORITY
usaf ltr, 28 feb 1972

SEISMIC DATA LABORATORY
QUARTERLY TECHNICAL SUMMARY REPORT
JANUARY - MARCH 1968

15 APRIL 1968

Prepared For

AIR FORCE TECHNICAL APPLICATIONS CENTER
Washington, D. C.

By

TELEDYNE, INC.

Under

Project VELA UNIFORM

Sponsored By

ADVANCED RESEARCH PROJECTS AGENCY
Nuclear Test Detection Office
ARPA Order No. 624

SEISMIC DATA LABORATORY
QUARTERLY TECHNICAL SUMMARY REPORT
JANUARY - MARCH 1968
15 APRIL 1968

AFTAC Project No.:	VELA T/6702
Project Title:	Seismic Data Laboratory
ARPA Order No.:	624
ARPA Program Code No.:	8F10
Name of Contractor:	TELEDYNE INDUSTRIES, INC.
Contract No.:	F 33657-68-C-0945
Date of Contract:	2 March 1968
Amount of Contract:	$ 1,251,000
Contract Expiration Date:	1 March 1969
Project Manager:	Royal A. Hartenberger (703) 836-7647

P. O. Box 334, Alexandria, Virginia

AVAILABILITY

This document is subject to special export controls and each transmittal to foreign governments or foreign nationals may be made only with prior approval of Chief, AFTAC. attn: VSC, Washington, D.C. 20333

The work reported herein was supported by the Advanced Research Projects Agency, Nuclear Test Detection Office, under Project VELA-UNIFORM and accomplished under the technical direction of the Air Force Technical Applications Center under Contract F 33657-68-C-0945.

ABSTRACT

This report summarizes the work done by the SDL during the period January through March 1968, and is primarily concerned with seismic research activities related to the detection and identification of nuclear explosions and earthquake phenomenon. Also discussed are the support tasks and data services performed for other participants in the VELA-Uniform project.

TABLE OF CONTENTS

LIST OF FIGURES

LIST OF TABLES

I. INTRODUCTION

This quarterly report summarizes the technical work, support effort, and service tasks completed during the period January through March 1968. Current or past work is mentioned only if it relates to the present discussions.

Reviews of technical reports completed during the reporting period are contained in Section II under descriptive headings. Section III is a summary of the support and service tasks performed for in-house projects and for other VELA-Uniform participants. This report concludes with Appendix A in which are listed the organizations who received SDL data services during the period.

II. WORK COMPLETED

A. LASA Travel-time Anomalies for 65 Regions Computed with the Herrin Travel-time Table, Nov. 1966 Version

A report was published concerning the results of computing P-wave relative travel-time anomalies at all subarray center instruments at the Large Aperture Seismic Array (LASA) in Montana. The travel-time table used for computing expected times is the Herrin, November 1966 version.

A total of 626 teleseisms are used. As the anomalies are dependent upon event distance and azimuth, all of the results are separated into groups such that the subarrays have anomalies which are consistent within each defined region.

The following description explains the presentation of the results in Figure 1 using the reference numbers below.

11 15 67 RELATIVE TRAVEL-TIME ANOMALIES

(1) HERRIN(1967) TABLES (3) INCLUDING ELLIPTICITY (2) REFERENCE STATION AB

(4) ANOMALY REGION = CENTRAL AND SOUTHERN ALASKA
DISTANCE RANGE = [illegible] KM AZIMUTH RANGE = 313.4 TO 320.0 DEGREES

(6)

(7) EVENT NAME	(8) DISTANCE	(9) AZIMUTH	(5) B1	(10) B2	B3	B4	C1	C2	C3	C4	D1	D2
19 AUG66 GULF ALASKA	2980.00	313.65	.047	.067	-.086	-.014	.129	.047	-.002	-.134	.107	.001
12 OCT 66 S ALASKA	2981.32	314.03	.047	.070	-.040	-.021	.153	.041	-.050	-.043	.045	.000
12 OCT 66 S ALASKA	2980.64	314.54	.101	.133	-.027	-.036	.202	.109	.037	.016	.191	.024
15 AUG66 NO ALASKA 1	2984.38	315.29	0	0	0	0	0	0	0	0	0	0
02 SEP66 SO ALASKA	3028.48	314.65	.128	.080	-.020	-.013	.164	.140	.007	0	.159	.030
09 APR66 SO. ALASKA	3039.38	314.61	.127	.061	-.110	-.032	-.007	.110	-.042	-.080	.188	.031
06 NOV65 S ALASKA	3059.03	315.42	0	0	0	-.057	.072	0	.017	-.046	.172	.070
30 AUG66 NO ALASKA	3080.18	314.85	.038	.079	-.024	-.001	0	.059	-.103	-.027	.052	-.022
30 AUG 66 S ALASKA	3091.18	317.27	.023	.099	-.038	-.021	0	.040	.091	-.020	-.049	0
22 JUN66 S. ALASKA	3099.10	317.02	0	0	-.116	-.037	-.052	.125	-.005	-.089	.041	.020
01 SEP66 SO ALASKA	3097.92	317.44	.056	.051	-.041	-.032	.017	.054	-.099	-.079	.080	0
15 AUG66 NO ALASKA	3115.74	314.14	.094	.103	0	-.049	.126	.127	0	-.044	.076	-.121
07 OCT 66 S ALASKA	3098.97	314.94	-.042	.002	-.016	-.125	.065	0	.018	-.041	.029	0
26 MAY 66 ALASKA	3267.19	314.17	0	-.005	-.020	.001	.162	.115	-.115	-.042	.006	-.014
19 MAR 66 CEN ALASKA	3300.19	313.16	-.031	-.057	-.041	-.031	.111	-.032	-.097	-.033	-.050	0
24 NOV65 C ALASKA	3310.26	310.90	.120	.003	0	-.029	.052	.048	-.090	-.089	.119	-.028
22 MAR66 SO. ALASKA	3320.60	315.64	.097	-.014	-.173	-.007	.062	.094	-.110	-.067	.137	-.128
04 FEB66 S. ALASKA	3327.32	314.20	.092	.048	.002	-.033	.018	-.035	-.039	.079	.178	-.003
06 FEB67 SOUTH ALASK	3351.54	313.55	.132	.020	-.092	-.027	.031	.098	-.040	-.026	.092	-.066
(13) AVERAGE			.070	.046	-.056	-.007	.082	.075	-.030	-.042	.074	-.020
(14) SIGMA			.055	.050	.054	.042	.071	.053	.047	.045	.071	.062
(15) N			19	16	15	18	16	16	17	17	16	12

EVENT NAME	DISTANCE	AZIMUTH	D3	D4	E1	E2	E3	E4	F1	F2	F3	F4
19 AUG66 GULF ALASKA	2980.00	313.65	-.177	.011	-.101	-.043	-.180	-.190	-.207	-.314	-.130	-.090
12 OCT 66 S ALASKA	2981.32	314.03	-.179	.002	-.123	-.014	-.159	-.193	-.010	-.305	-.190	.009
12 OCT 66 S ALASKA	2980.64	314.54	-.156	.070	0	-.071	0	-.209	-.117	-.192	-.119	-.039
15 AUG66 NO ALASKA 1	2984.38	315.29	0	0	0	0	-.192	-.164	-.112	-.230	-.145	-.111
02 SEP66 SO ALASKA	3028.48	314.65	-.086	.006	0	-.037	0	-.209	-.146	-.221	-.024	-.002
09 APR66 SO. ALASKA	3039.38	314.61	-.155	.043	0	-.048	-.032	-.307	-.008	-.324	-.098	0
06 NOV65 S ALASKA	3059.03	315.42	-.116	.012	0	0	0	-.145	-.076	-.188	0	-.160
30 AUG66 NO ALASKA	3080.18	314.85	-.094	.032	-.266	-.097	-.121	-.076	-.094	-.158	-.007	-.222
30 AUG 66 S ALASKA	3091.18	317.27	-.119	-.022	-.320	-.106	-.140	-.306	-.188	-.337	-.069	-.412
22 JUN66 S. ALASKA	3099.10	317.02	-.100	.001	-.170	-.114	-.038	-.157	-.022	-.175	-.078	-.149
01 SEP66 SO ALASKA	3097.92	317.44	-.185	0	-.208	-.088	-.177	-.150	-.059	-.386	-.163	-.254
15 AUG66 NO ALASKA 2	3115.74	314.14	0	-.109	0	0	0	-.330	0	-.432	0	-.196
07 OCT 66 S ALASKA	3098.97	314.94	-.038	-.158	-.190	-.134	-.214	-.225	-.067	-.358	-.289	-.122
26 MAY 66 ALASKA	3267.19	314.17	-.177	-.011	-.198	-.075	-.001	-.160	-.131	-.341	-.123	-.228
19 MAR 66 CEN ALASKA	3300.19	313.16	-.221	-.158	0	-.057	-.011	-.292	-.045	-.399	0	-.492
24 NOV65 C ALASKA	3310.26	310.90	-.104	.001	-.043	-.002	0	-.188	-.032	-.183	-.098	0
22 MAR66 SO. ALASKA	3320.60	315.64	-.153	.013	0	0	0	0	0	0	0	0
04 FEB66 S. ALASKA	3327.32	314.20	-.113	-.010	-.084	-.033	-.224	-.245	-.025	-.328	-.091	-.091
06 FEB67 SOUTH ALASK	3351.54	313.55	-.062	.005	-.183	-.039	-.114	-.193	-.131	-.259	-.084	-.172
AVERAGE			-.147	.007	-.164	-.010	-.136	-.203	-.061	-.278	-.083	-.172
SIGMA			.076	.072	.083	.074	.084	.060	.076	.090	.081	.122
N			17	17	11	15	13	10	17	16	15	16

EVENT PARAMETERS

(16) 19 EPICENTERS	(17) LATITUDE	(18) LONGITUDE	(19) DEPTH	(20) ORIGIN TIME	(21) SHOCK SIGMA	(22) AV. ERROR	(23) NO. STA
19 AUG66 GULF ALASKA	59.500	-144.600	33	03 10 04.8	.0577	-.002	20
12 OCT 66 S ALASKA	60.500	-144.400	33	03 19 25.4	.0520	.011	10
12 OCT 66 S ALASKA	60.400	-145.000	25	08 24 30.0	.0602	.046	14
15 AUG66 NO ALASKA 1	60.400	-144.000	0	13 36 22.7	.0567	-.002	6
02 SEP66 SO ALASKA	60.200	-146.900	31	22 46 39.5	.0400	.042	17
09 APR66 SO. ALASKA	60.200	-147.100	34	18 51 45.8	.0674	.016	10
06 NOV65 S ALASKA	60.400	-147.300	37	06 38 41.5	.0878	.052	12
30 AUG66 NO ALASKA	61.300	-147.500	36	20 20 54.8	.0643	.006	19
30 AUG 66 S ALASKA	61.500	-147.500	33	20 23 18.8	.0821	-.030	10
22 JUN66 S. ALASKA	61.400	-147.700	33	11 30 53.7	.0670	.019	10
01 SEP66 SO ALASKA	61.900	-149.600	77	23 19 00.2	.0503	-.026	16
15 AUG66 NO ALASKA 2	61.200	-150.000	98	19 37 16.0	.0816	-.024	12
07 OCT 66 S ALASKA	61.600	-150.100	54	20 05 56.0	.0962	-.052	10
26 MAY 66 ALASKA	60.800	-151.000	94	10 44 13.0	.0606	-.007	19
19 MAR 66 CEN ALASKA	62.300	-151.200	87	09 33 43.2	.1092	-.064	17
24 NOV65 C ALASKA	63.200	-151.800	129	00 22 38.7	.0561	.000	17
22 MAR66 SO. ALASKA	61.100	-152.000	108	10 28 58.0	.0575	-.024	12
04 FEB66 S. ALASKA	60.400	-152.300	91	23 20 07.0	.0601	.016	20
06 FEB67 SOUTH ALASK	60.100	-152.800	110	03 26 35.4	.0446	.000	20

Figure 1. RELATIVE TRAVEL-TIME ANOMALIES

1. Source of expected travel times. In this report, the Herrin table, November 1966 version, is used;

2. Reference subarray, R, selected for computing relative anomalies. In this report, all anomalies are relative to subarray A0. The following relation may be used to change reference stations;

$$A_{i/j} = A_{i/r} - A_{j/r}$$

where $A_{i/j}$ is the anomaly at station i relative to a new reference station j.

3. All expected travel-times in this report have been corrected for the ellipticity of the earth such that the computed anomalies may be used in conjunction with other programs requiring these corrections.

4. An arbitrary geographic name given to the event region.

5. Range of epicentral distance in the event region.

6. Range of epicentral azimuth in the event region.

7. Date and arbitrary name given to each event.

8. Epicentral distance, in kilometers, from the reference subarray, R.

9. Epicentral azimuth, in degrees measured from north to east, from the reference subarray, R.

10. Subarray designator, i.

11. Measured travel-time anomaly, in seconds, at subarray i relative to subarray R for the kth event;

$$A^k_{i/r} = T^k_i - T^k_r - H^k_i + H^k_r$$

where T is the observed arrival time and H is the expected

(Herrin 1966) travel time from the hypocenter of the kth event including correction for ellipticities but <u>not</u> for station elevations.

12. A fixed-point zero anomaly indicates that no reading was made at the subarray for that event.

13. The average anomaly at subarray i of N recorded events;

$$\bar{A}_{i/r} = \left(\sum_{k=1}^{N} A^{k}_{i/r} \right) /N$$

for the defined region.

14. Standard deviation, or error of estimate, at the ith subarray for N observations:

$$\sigma_i = \left\{ \left[\sum_{k=1}^{N} (A^{k}_{i/r} - \bar{A}_{i/r})^2 \right] /(N-1) \right\}^{\frac{1}{2}}$$

for the defined region.

15. Number of observations, N, at station i for the defined region.

16. Total number of epicenters included in the defined region.

17. Epicenter latitude, degrees (USC&GS); plus north, minus south.

18. Epicenter longitude, degrees (USC&GS); plus east, minus west.

19. Event depth, kilometers (USC&GS).

20. Event origin time, hours, minutes, seconds (USC&GS).

21. Standard deviation, or error of estimate, of the kth event in the defined region;

$$\sigma_k = \left\{ \left[\sum_{i=1}^{L} (A^k_{i/r} - \bar{A}_{i/r})^2 \right] / (L-1) \right\}^{\frac{1}{2}}$$

where L is the number of subarrays recording the kth event not including the reference subarray R.

22. Average error, or bias, of the kth event;

$$E_k = \sum_{i=1}^{L} (A^k_{i/r} - \bar{A}_{i/r})/L$$

where L is the number of subarrays recording the kth event not including the reference subarray R.

23. Number of subarrays, L, recording the kth event, not including the reference subarray R.

The results in Report 204 are arranged first by general direction (beginning with the northwest and going clockwise and second by increasing epicentral distance within each directional group (See Table 1).

The following observations similar to those in a previous report using the Jeffreys-Bullen travel-time tables (Chiburis, 1966), are made concerning the LASA travel-time anomalies using the Herrin, November 1966 tables:

1. The anomaly variations between regions measured at a single subarray are as high as 1.66 seconds. For example, subarray F4 has an average anomaly of +0.74 sec (N = 19, $\sigma_{F4} = 0.13$) for the No. Colombia region and an average of -0.92 sec (N = 12, $\sigma_{F4} = 0.07$) for the Solomon Is. region.

2. Subarrays which are quite near the reference subarray A0 can have unusually large anomalies. For example, subarray D4 is located 30.75 km from A0 (center instrument to center instrument) and has an anomaly relative to A0 of +0.83 sec. (N = 7, $\sigma_{D4} = 0.06$) for the Dominican Republic-Mona Passage region.

TABLE I

Distance-azimuth ranges by region

Direction	No. of Regions	Distance Range, km	Azimuth Range, deg	No. of Events
Northwest	15	2800-10900	292-329	214
North	6	5300-11000	340-016	36
Northeast	9	4700-10700	018-071	65
East	4	5700- 9900	075-103	16
East-southeast	3	4500- 5800	112-121	23
Southeast	13	3100-10800	132-170	133
South	8	2200-10100	158-192	49
Southwest	2	9500-10900	238-248	43
West	2	10600-11100	259-274	20
Undefined	3			
Continental U.S.		683- 2900	101-281	7
Eastern Is. and Pacific Ocean		4400-10800	184-253	6
Miscellaneous		2100-9600	334-007	14

3. The center instrument at subarray B2 is only 7.50 km from the center at A0, but it has an anomaly of -0.30 sec (N = 13, σ_{B2} = 0.04) for the Yugoslavia-Albania-Greece-Mediterranean Sea Region. This result suggests that the time anomalies within one subarray (7 km diameter) are far from negligible. Signals recorded within a subarray can be significantly misaligned with anomalies as large as 0.30 sec.

4. The anomalies are not slowly varying functions of either distance or azimuth. For example, subarray F1 has an anomaly of +0.22 sec (N = 7, σ_{F1} = 0.09) computed from events approaching from an east-southeastly direction at 5100 km distance (Virgin-Leeward Is. region), but at 4600 km (Dominican Republic-Mona Subarray F2, on the other hand, has an anomaly of +0.12 sec (N = 6, σ_{F2} = 0.08) for events bearing 145° at 4800 km (So. Central America), whereas for events bearing 113° at a distance of 5100 km (Virgin-Leeward Is. region) the anomaly is -0.57 sec (N = 6, σ_{F2} = 0.06). Hence, the anomaly at F1 changes by 0.62 sec in a distance range of 500 km, and at F2 it changes by 0.69 sec in an azimuth range of 32°.

5. The maximum anomaly range observed at LASA is 1.94 sec; average anomaly at subarray F2 is -1.01 sec for events occurring in Rumania; average anomaly at subarray E1 is +0.93 for events from the No. Colombia region.

6. The maximum anomaly range for one particular region (North Atlantic Ridge) is 1.43 sec, where the D4 anomaly is +0.47 sec and the F2 anomaly is -0.97.

Reference

Chiburis, E.F., 1966, "LASA Travel-Time Anomalies for Various Epicentral Regions", Seismic Data Laboratory Report No. 159, 13 September.

B. Lateral Variations in Crustal Structure Beneath the Montana LASA

The analysis of a variety of geologic and geophysical data indicates that significant lateral variations in crustal structure exist across LASA. This structural complexity is inferred from observation of Rayleigh wave dispersion, body-wave spectral ratios, P-wave amplitude and travel-time anomalies, seismic refraction profiles and gravity and magnetic anomalies. To explain these results, LASA is divided into an eastern and a western sector. An attempt is made to explain the observations in each sector in terms of crustal models consisting of 3 to 5 distinct layers. The observations show that the maximum lateral change in structure across LASA takes place in a NE-SW direction.

The most striking feature of the evidence presented is its consistency. The repeated appearance of the NW-SE trend suggests that this is fundamental to the structure beneath the array. Only in the distribution of travel-time anomalies is it not readily discernible. In the following discussion we shall attempt to explain our observations in terms of a model which may form the basis for future investigations.

From the Rayleigh wave dispersion data, supplemented by the evidence from the spectral ratios and the aeromagnetic map, it is evident that as a starting point LASA may be divided into two sectors by the line A-A' (See Figure 2). To the east of

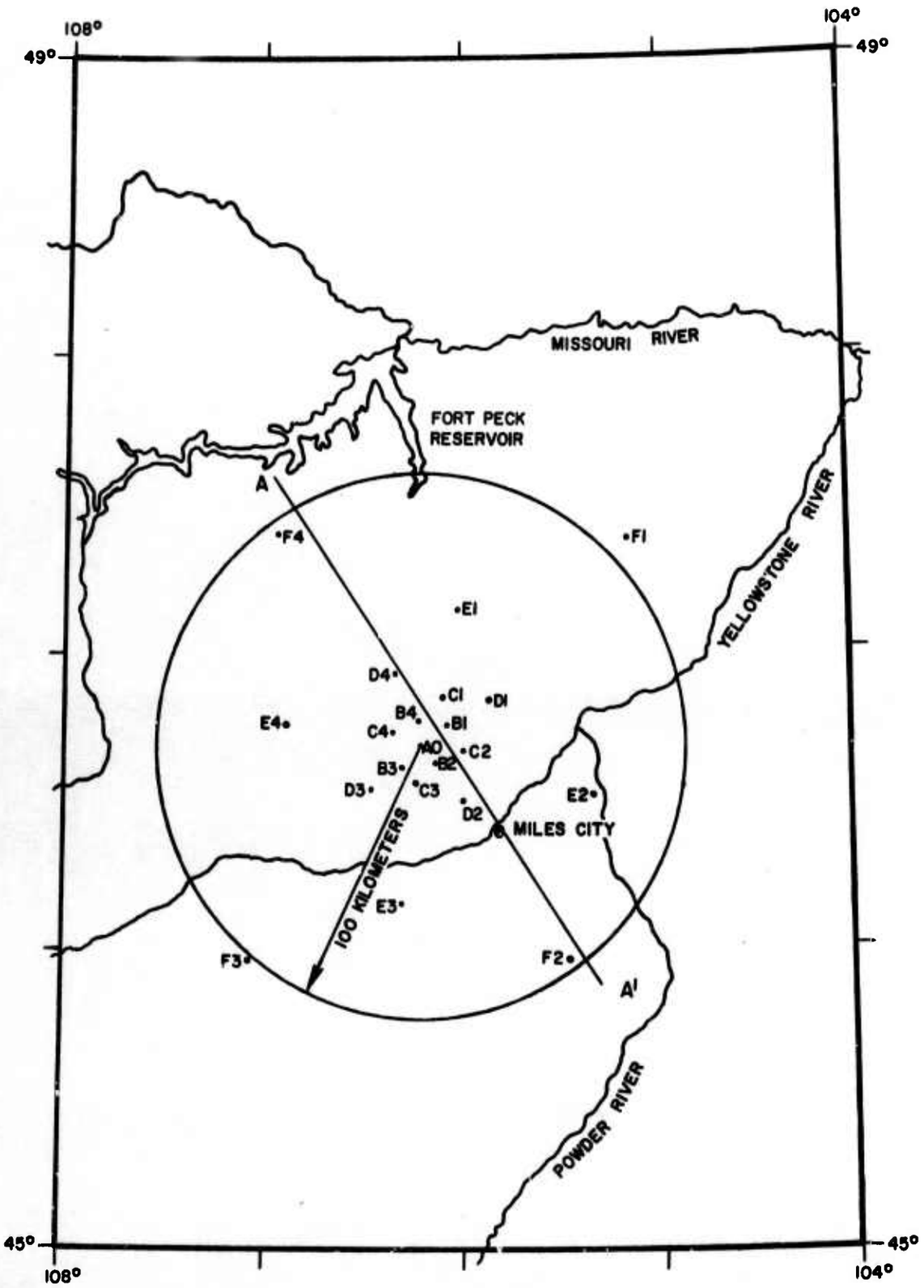

Figure 2. Location of the Montana LASA

of this line the observed phase velocities are higher than those to the west. Of the crustal models considered, U.W.3 best fits the observed data for the eastern sector, whereas USGS3 best fits the observed data for the western sector of LASA. Some important implications of this division are:

1. Seismic velocities in the eastern sector are significantly higher than those in the western sector;

2. The total thickness of the crust is greater in the east than in the west;

3. The models indicate a reduction in the number of major layers within the basement, from three in the east to two in the west.

The observed decrease in phase velocities to the west of A-A' is in apparent contradiction to the overall reduction in thickness of the crust inferred from the seismic refraction results. To explain this it is necessary to postulate the presence either of dipping layers within the crust, or lateral changes in velocity within particular layers, or both. Dipping layers have been identified in the seismic refraction studies (See Figures 3 and 4); furthermore, the implied reduction in the number of layers within the basement may be explained in this manner.

The nature of the boundary between the two sectors is problematical. The geologic data do not indicate the presence of large fault or fault zone within the sedimentary sequence (i.e., the uppermost 3 km) of the crust. This is emphasized by the dispersion results, which indicate that the amount of lateral refraction which Rayleigh waves undergo on crossing LASA

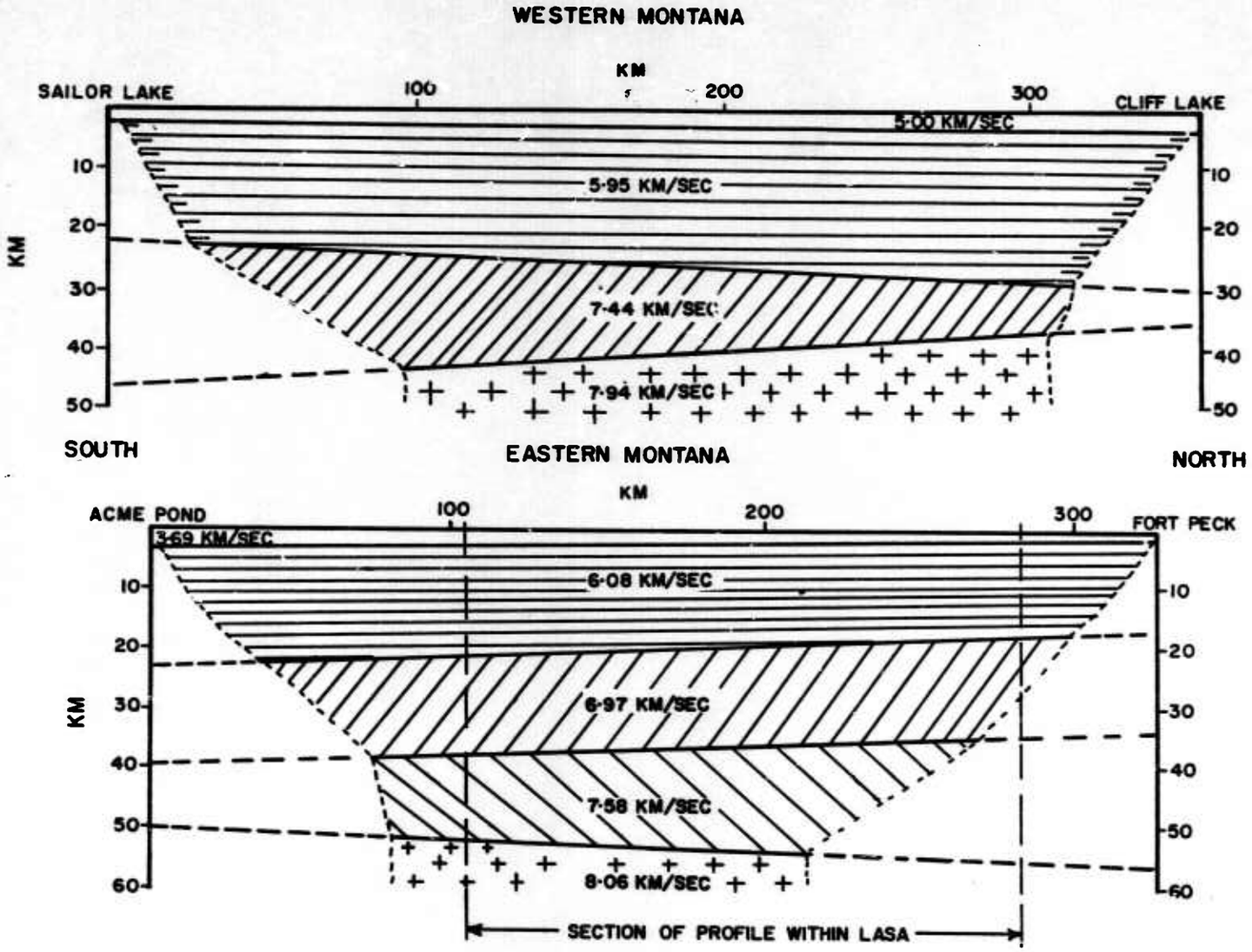

Figure 3. The University of Wisconsin Crustal Models.
(After Meyer et al, 1961)

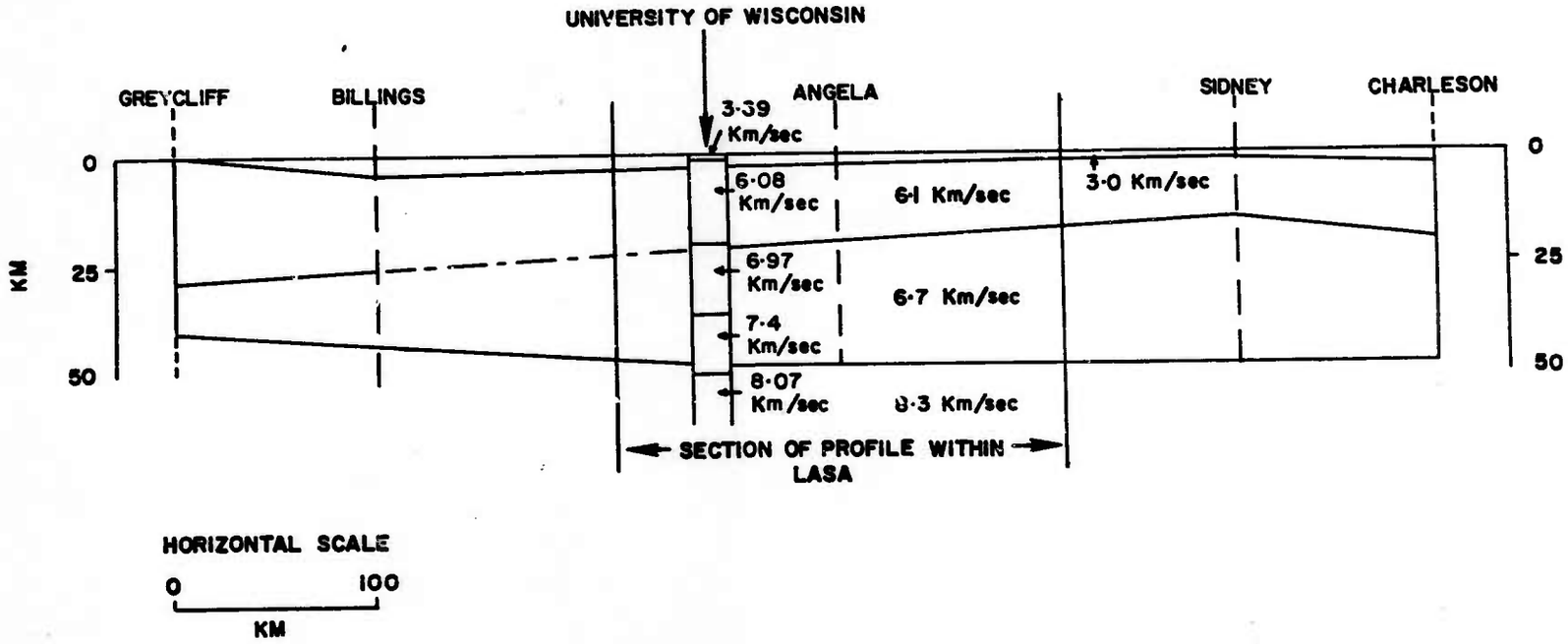

Figure 4. The USGS Crustal Model. (After Borcherdt and Roller, 1967)

increases with depth, at least to about 50 km. This implies that the boundary lies at some depth within the crust, as has been postulated by Zeitz (personal communication, 1967) on the basis of the magnetic data.

Moreover, it is possible that the boundary is gradational rather than abrupt. The dispersion results indicate only that a change takes place. We must await the detailed interpretation of the gravity and magnetic maps before speculating on the nature of the boundary itself.

So far we have sought only to explain the dispersion results. The travel-time anomalies must also be explained in terms of a crustal model. Of the explanations put forward to date, three will be discussed here; bearing in mind that any explanation must satisfactorily account for the "synclinal" feature reported by Sheppard (1967) and substantiated by our results.

To explain the synclinal feature Sheppard (1967) has proposed two alternate hypotheses. They are:

1. A relative thickening of the earth's crust by some 10 km under subarray B4 with respect to F2 and F4. This would correspond to a five-degree to six-degree slope in the Moho from F4 to F2 and from F2 to B4.

2. A thickening of the 3.0 km/sec (sedimentary) layer by 3 km under subarray B4.

Neither of these hypotheses are supported by our results. If the Moho dips by as much as 5 degrees then the division of the array into northern and southern sectors should yield relatively lower phase velocities in the north compared to the south, for the Greenland Sea event. As was indicated previously, the

phase velocities for the southern sector were higher than those for the northern sector. Also the division of LASA into an inner and outer group of subarrays indicated no strong thickening under the center of the array. From a consideration of the well log data and from the geologic sections presented by Brown and Poort (1965), there is no evidence to suggest an increase of 3 km (nearly 100%) in the sedimentary sequence anywhere under LASA.

The third hypothesis, proposed by Fairborn (1966), suggests that the azimuthal dependency of the travel-time anomalies requires horizontal velocity gradients in the crust and upper mantle. Our data and Sheppard's (1967) indicates that horizontal velocity gradients are insufficient in themselves to account for the observed anomalies. Both the seismic refraction data and the Rayleigh wave dispersion data indicate that the average velocity of a 55 km-thick section under LASA decreases from east to west. Such a decrease in velocity would result in systematically later arrivals towards the west of the array if horizontal velocity gradients alone are responsible for the observed travel time anomalies. From our observations and Sheppard's, the later arrivals define a "synclinal" feature to the NE of A0. This suggests that two of the more important factors bearing on the distribution of the observed travel time anomalies are:

1. dipping layers within the crust;
2. the pre-Cretaceous structure of the Paleozoic rocks and possibly the upper part of the basement also.

Moreover, since large amplitudes are consistently recorded at the center of LASA, it seems that the anticlinal structures which surround the array give rise to a lens effect which results in the focusing of body waves toward the center of the array. However, more observations are needed to substantiate that this occurs.

From the analysis of the geologic and geophysical data we conclude:

1. Lateral variations exist in the structure of the earth's crust beneath LASA. The geologic, aeromagnetic and surface wave dispersion data show that this variation is within the basement at a depth greater than three kilometers. The maximum change takes place in a NE-SW direction (i.e., perpendicular to the dominant NW-SE structural trend).

2. The observations are best explained by dividing LASA into an eastern and a western sector by a line trending N20°W through Miles City, Montana. For the eastern sector, the average seismic velocities of the crust are higher, the crust is thicker, and Model U.W.3 best accounts for the observed dispersion. For the western sector, the velocities are lower, the crust is thinner, and model USGS3 best accounts for the observed dispersion results.

3. The individual layers within the crust are dipping, though not in the same direction.

To refine the model further it is recommended that:

1. The individual travel-time anomalies at each station be obtained as a function of distance and azimuth;

2. More events be examined. In particular, more spectral ratios must be obtained to determine an average structure under each subarray and then Rayleigh waves from events at more azimuths and distances should be analyzed to establish better the attitude and thickness of the intermediate crustal layers.

References

Aldrich, L.T. and M.A. Tuve, Crustal structure in the Rocky Mountains; Part I: Observation of the University of Wisconsin shots by the Carnegie Institution of Washington, paper presented at the meetings of the IUGG, July, 1960.

Alexander, S.S., Surface wave propagation in the Western United States, Ph.D. thesis, California Institute of Technology, Pasadena, 1963.

Anon., Unpublished company memorandum on LASA, Earth Sciences, Teledyne, Inc., Pasadena, 3 pp., 1965.

Asada, Toshi, and L.T. Aldrich, Seismic observations of explosions in Montana, in The Earth beneath the Continents, Geophys. Monograph 10, edited by J.S. Steinhart and T.J. Smith, pp. 382-390, American Geophysical Union, Washington, D.C. 1967.

Borcherdt, C.A., and J.C. Roller, Preliminary interpretation of a seismic-refraction profile across the Large Aperture Seismic Array, Montana, USGS Tech. Letter No. NCER-2, U.S. Geological Survey, Melno Park, 31 pp., 1967.

Brown, T.G., and J.M. Poort, Subsurface studies and shallow-hole preparation LASA area, Eastern Montana, Tech. Rep. No. 65-21, The Geotechnical Corp., Garland, 14 pp., 1965.

Brune, J., and J. Dorman, Seismic waves and earth structure in the Canadian Shield, Bull. Seismol. Soc. Am., 53, 167-201, 1963.

Chiburis, E.F., LASA travel-time anomalies for various epicentral regions, Seismic Data Laboratory Report No. 159, 1966.

Cooley, J.W. and J.W. Tukey, An algorithm for the machine calculation of complex Fourier series, Math. Computation, 19, 297-301, 1965.

Evernden, J.F., Direction of approach of Rayleigh waves and related problems, Part I, Bull. Seismol. Soc. Am., 43, 335-374, 1953.

Fairborn, J.W., Station corrections at LASA, AFOSR Contract, Department of Geology and Geophysics, Massachusetts Institute of Technology, Cambridge, 16 pp., 1966.

Harkrider, D.G. and D.L. Anderson, Computation of surface wave dispersion for multilayered anisotropic media. Bull. Seismol. Soc. Am., 52, 321-332, 1962.

Hasdell. N.A., The dispersion of surface waves of multilayered media, Bull. Seismol. Soc. Am., 43, 17-34, 1953.

James, D.E., and J.S. Steinhart, Structure beneath continents: A critical review of explosion studies 1960-1965, in The Earth beneath the Continents, Geophys. Monograph 10, edited by J.S. Steinhart and T.J. Smith, pp. 293-333, American Geophysical Union, Washington, D.C., 1967.

Klappenberger, F.A., Spatial correlation of amplitude anomalies, Seismic Data Laboratory Report No. 195, 8 pp., 1967.

McCamay, Keith, and R.P. Meyer, A correlation method of apparent velocity measurement, J. Geophys. Res., 69, 691-699, 1964.

McCowan, D.W., Finite Fourier transform theory and its application to the computation of convolutions, correlations, and spectra, Seismic Data Laboratory Report No. 168 (Revised), 1967.

McCowan, D.W., Design and evaluation of certain multichannel filters, Seismic Data Laboratory Report No. 209, 31 pp, 1968.

Meyer, R.P., J.S. Steinhart, and W.E. Bonini, Montana, 1959, in Explosion Studies of Continental Structure, Publication No. 622, edited by J.S. Steinhart and R.P. Meyer, pp. 305-343, Carnegie Institution of Washington, Washington, D.C. 1961.

Miller, M.K., A.F. Linville, and H.K. Harris, Continuation of basic research in crustal studies, Final Report AFOSR 67-1581, Texas Instruments, Inc., Dallas, 116 pp., 1967.

Phinney, R.A., Structure of the Earth's crust from spectral behavior of long-period body waves, J. Geophys. Res., 69, 2997-3017, 1964.

Sheppard, R.M., Values of LASA time stations residuals, velocity and azimuth errors, Technical Note 1967-44, Lincoln Laboratory, Massachusetts Institute of Technology, Lexington, 95 pp., 1967.

Smith, J.G., Fundamental transcurrent faulting in Northern Rocky Mountains, A.A.P.G. Bull, 49, 1398-1409, 1965.

Steinhart, J.S., and G.P. Woollard, Seismic evidence concerning continental crustal structure, Explosion studies of Continental Structure, Publication No. 622, edited by J.S. Steinhart and R.P. Meyer, pp. 345-383, Carnegie Institution of Washington, Washington, D.C. 1961

Stoneley, R., On the apparent velocity of earthquake waves over the surface of the earth, Mon. Not. Roy. Astron. Soc. Geophys. Suppl., 3, 262-271, 1935.

C. High-Resolution Frequency-Wavenumber Spectra

Burg (1967) has shown that high-resolution power spectra can be computed from relatively short correlation functions by first least-squares predicting larger correlation lags from those already known. The resulting high-resolution power spectrum is inversely proportional to the power spectrum of the corresponding prediction error operator. However, with the advent of the Cooley-Tukey fast Fourier transform algorithm and related methods for estimating power spectra, the high-resolution technique for ordinary power spectra is no longer economical. It is now feasible

to compute power spectra as if they were Fourier transforms of the 100%-lag correlation functions; various kinds of smoothing can then be applied to reduce the spectra to the desired length and stability.

We feel that the most promising application of the high-resolution procedure lies in estimating frequency-wavenumber spectra. Here the length of the spatial correlation functions, which ultimately determines the resolution, is limited by the size of the array. The high resolution method is therefore the appropriate way to obtain frequency-wavenumber spectra which are sharp in wavenumber space from data recorded over small arrays.

It should be noted that computing high-resolution frequency-wavenumber spectra with our method is only negligibly more expensive than computing ordinary frequency-wavenumber spectra. Both techniques require computing the spectral matrix. The only other computations required by the high-resolution technique are the addition of some white noise, one Hermitian matrix inversion, and one Hermitian matrix multiplication.

Two events and samples of noise immediately preceding them were selected as examples of high-resolution frequency-wavenumber data processing. The first event and its corresponding noise sample were used to illustrate the application of the technique to a two-dimensional surface array, in this case the WMSO array, while the remaining data were used to illustrate results from a one-dimensional vertical array, the APOK deep well.

Ordinary frequency-wavenumber spectra of both pairs of noise samples and signals are shown in Figures 5, 7, 9a and 10a. Figures 5 and 9a are the noise samples and Figures 7 and 10a are the signals. The WMSO noise seems to be coming from the

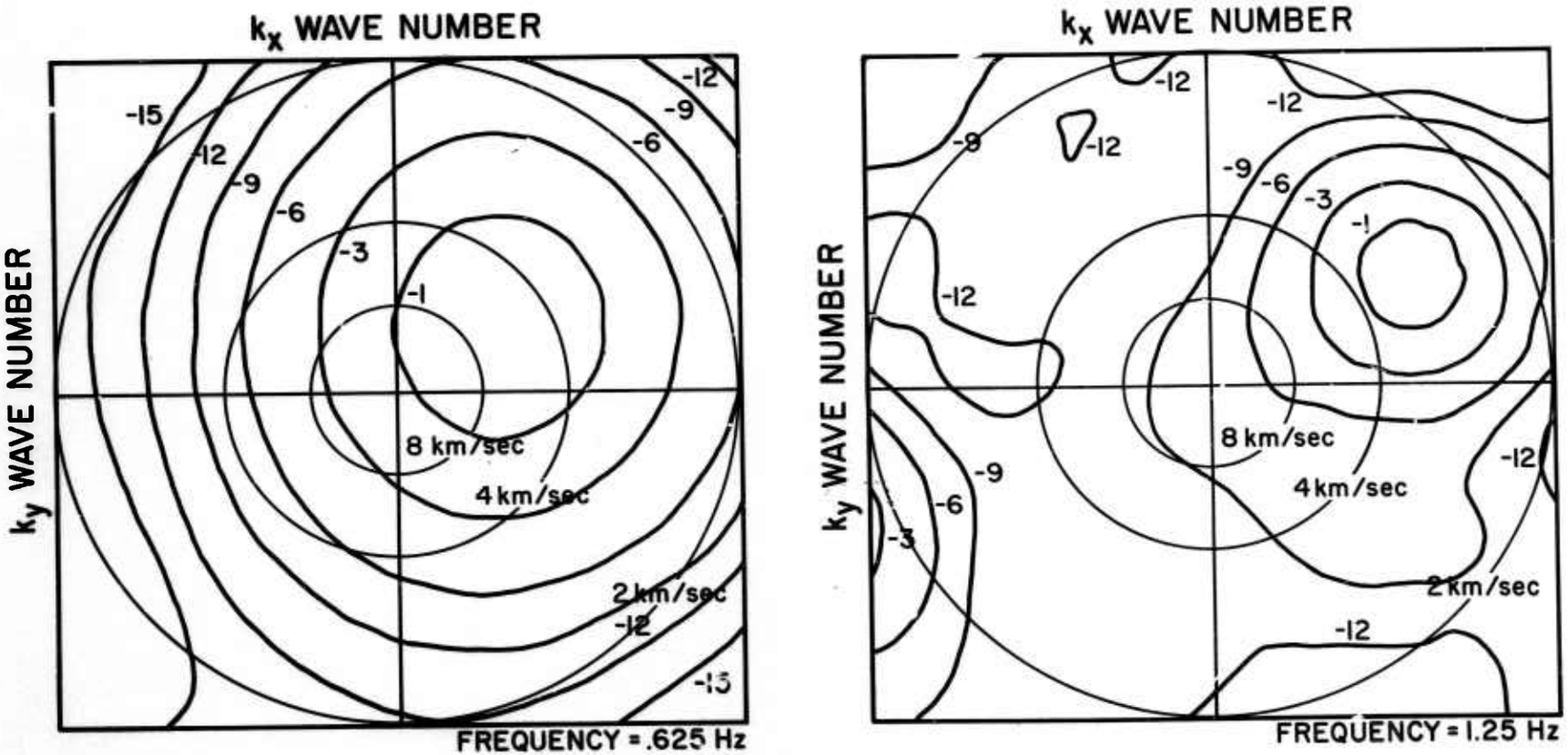

Figure 5. Ordinary frequency-wavenumber spectra of WMSO noise

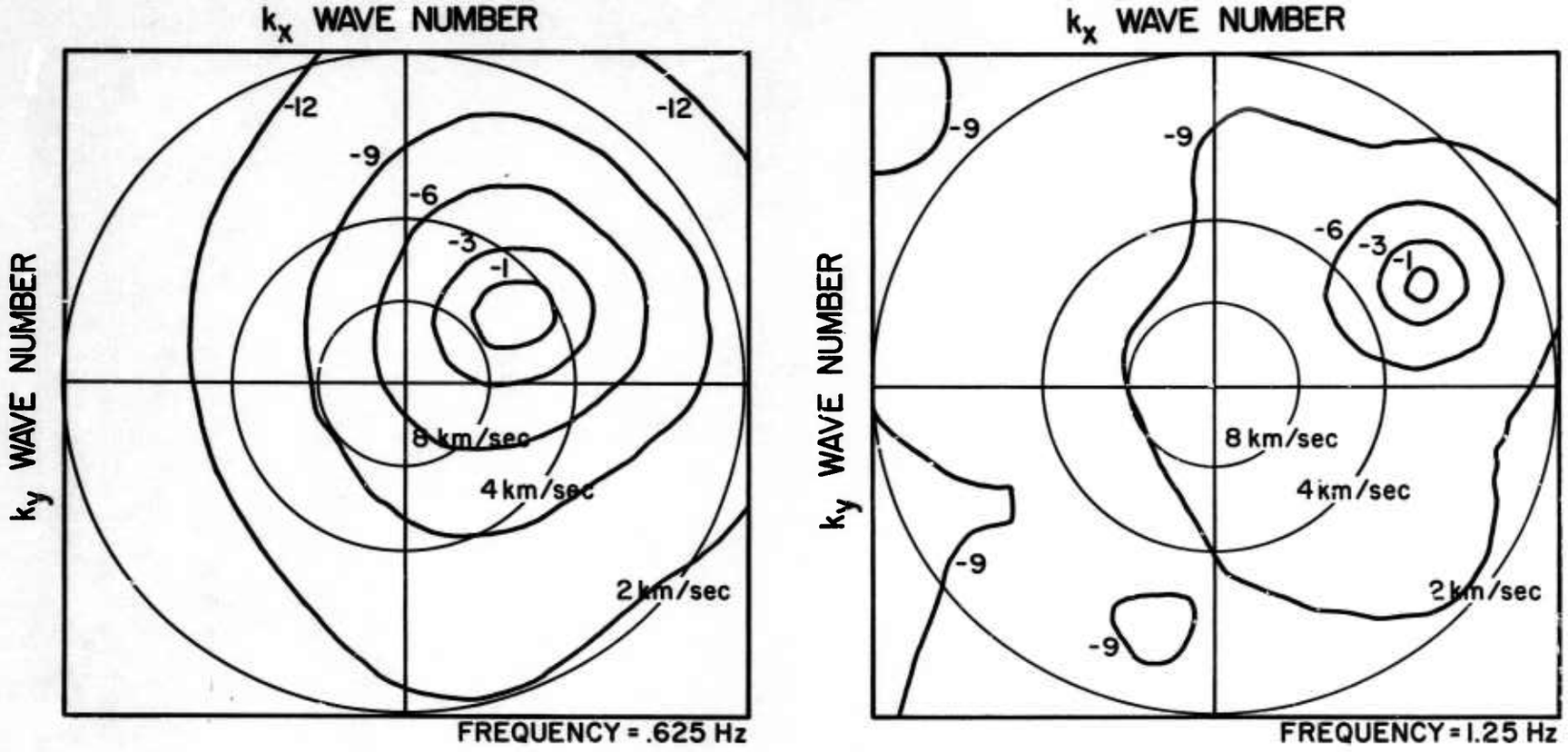

Figure 6. High-resolution frequency-wavenumber spectra of WMSO noise

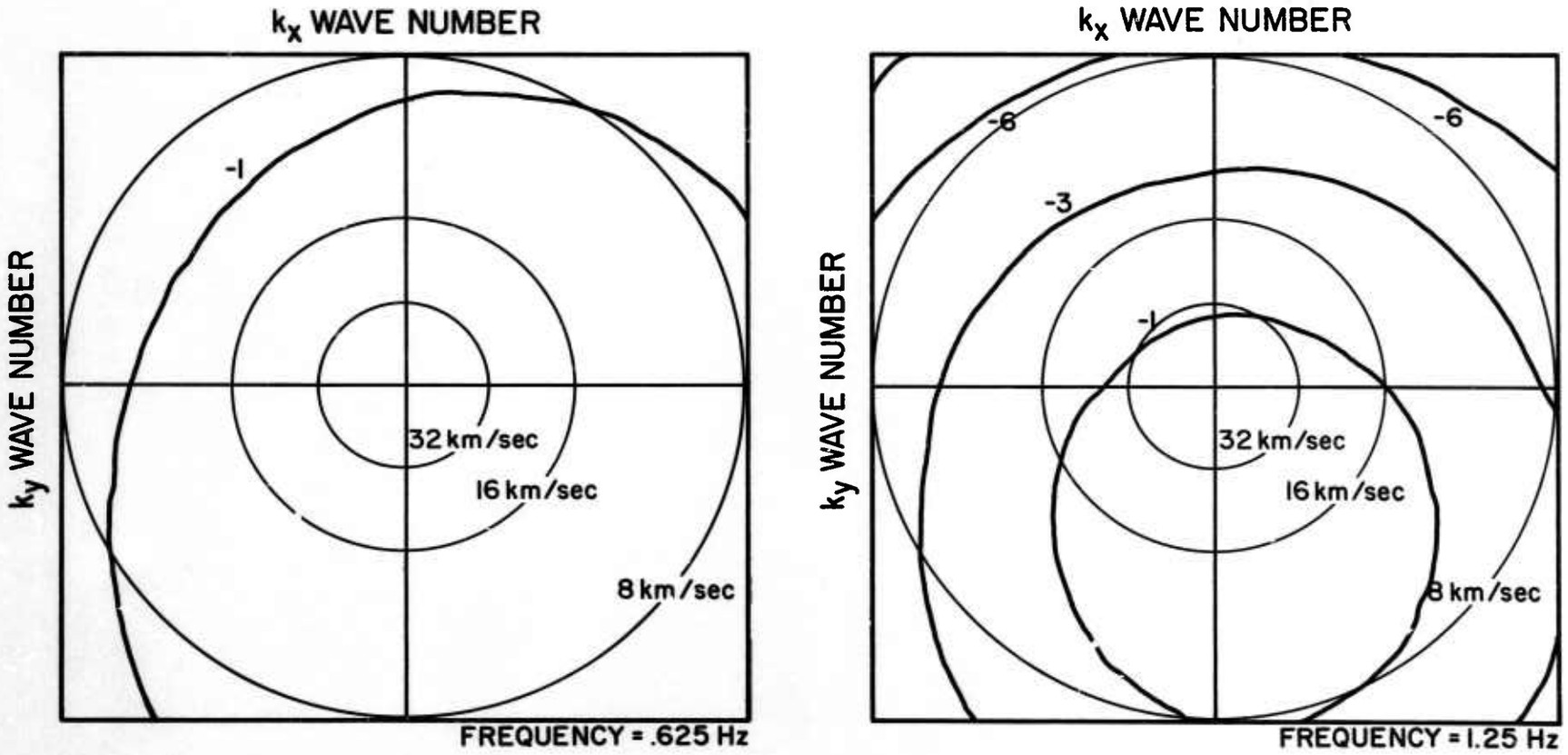

Figure 7. Ordinary frequency-wavenumber spectra of a WMSO signal

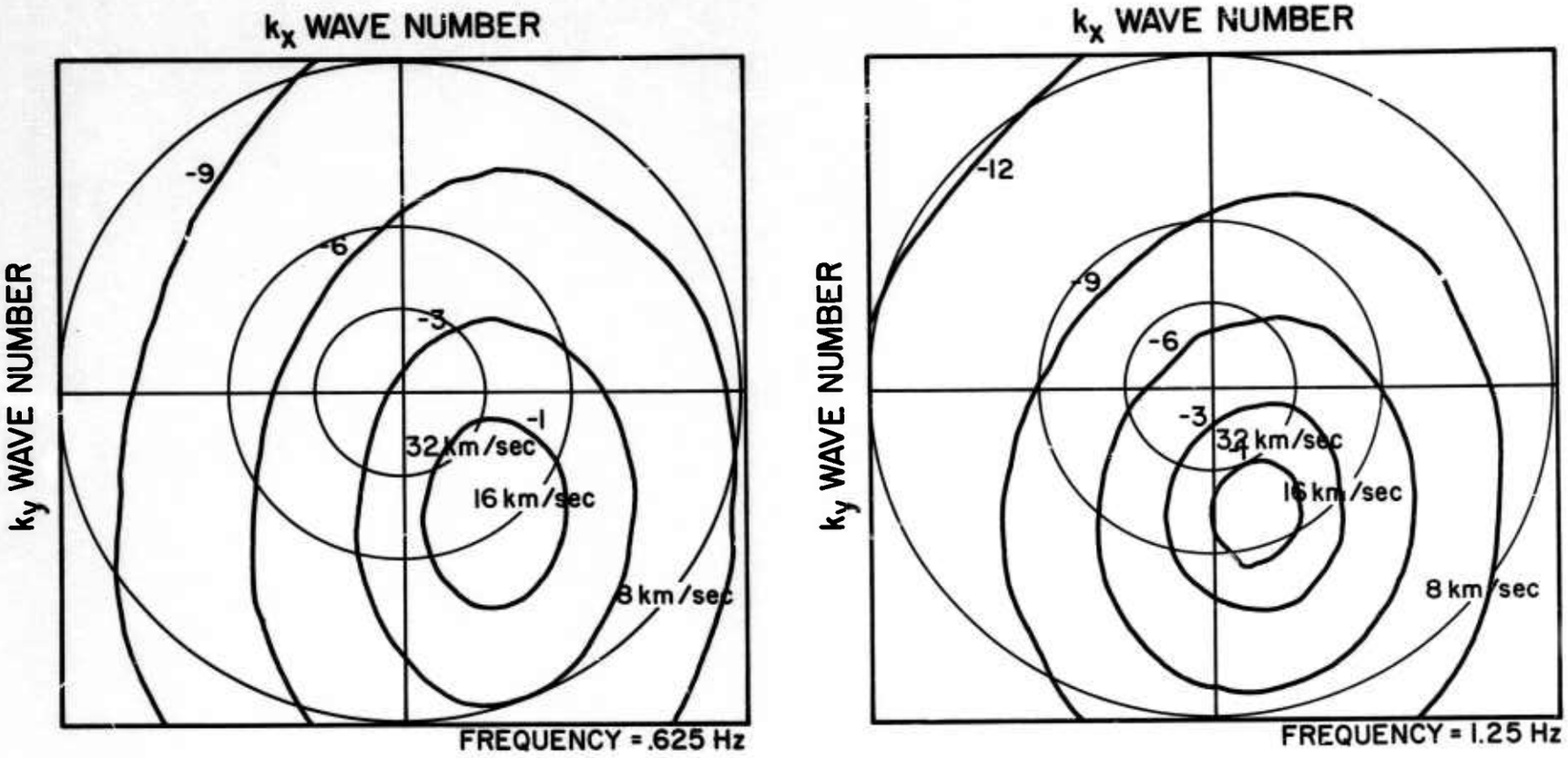

Figure 8. High-resolution frequency-wavenumber spectra of a WMSO signal

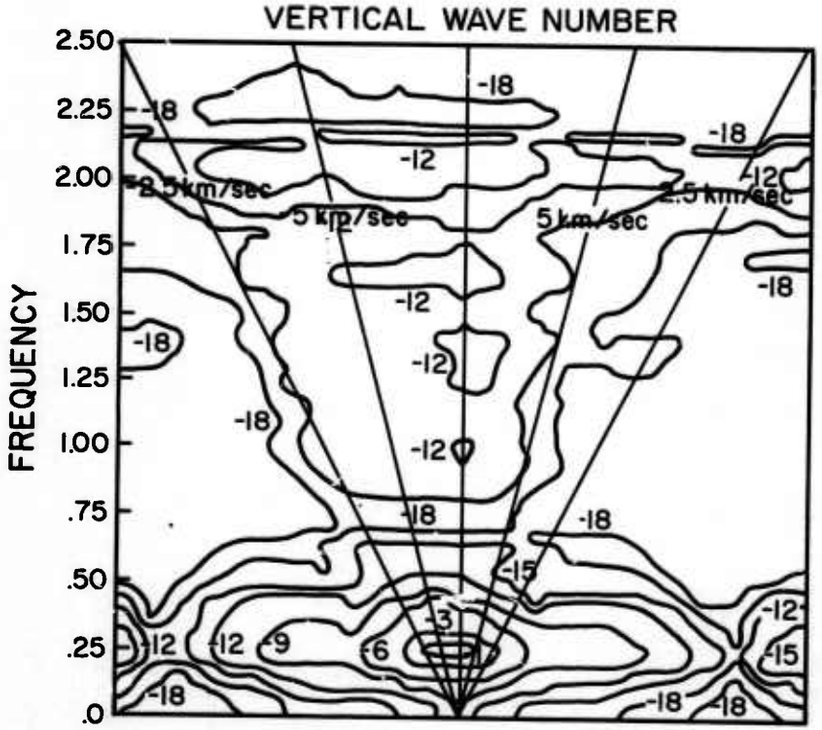

Figure 9a. Ordinary frequency-wavenumber spectrum of APOK noise

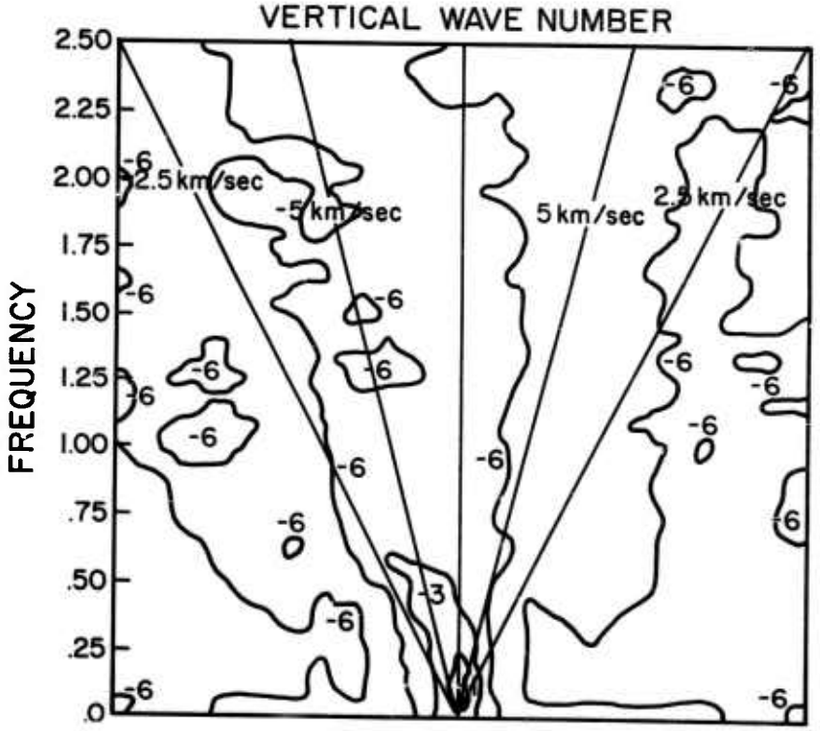

Figure 9b. High-resolution frequency-wavenumber spectrum of APOK noise

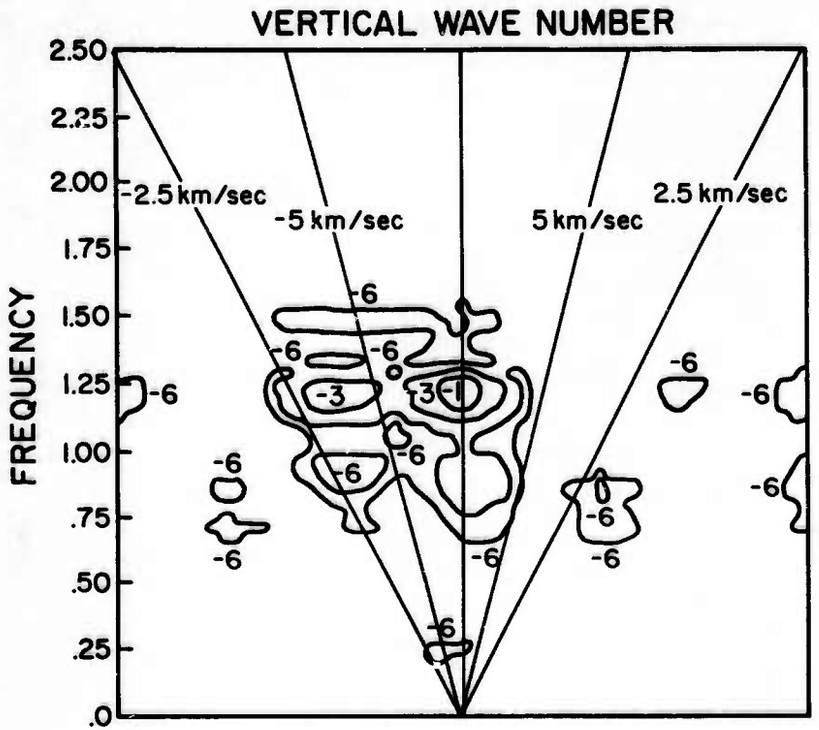

Figure 10a. Ordinary frequency-wavenumber spectrum of an APOK signal

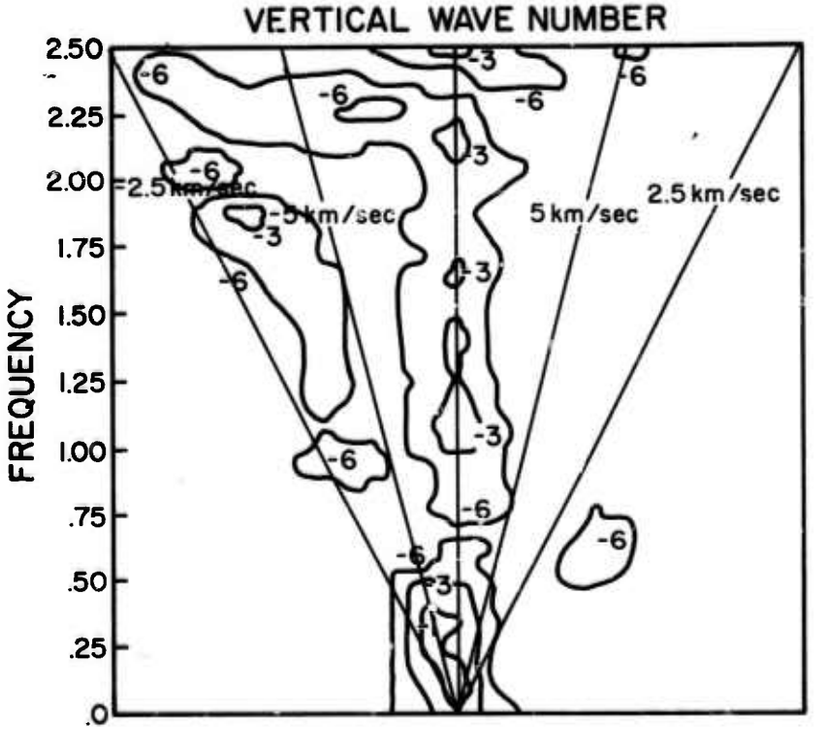

Figure 10b. High-resolution frequency-wavenumber spectrum of an APOK signal

northeast with a velocity ranging between 3 and 6 km/sec. This characteristic behavior has been noted by other investigators (Rizvi et al., 1967). On the other hand, the WMSO signal appears to be coming from the south or southeast with a velocity somewhere between 16 and 20 km/sec. The APOK noise sample displays a tilted pattern also characteristic of the site. One explanation for this phenomenon is suggested by the geological structure in the vicinity of the well (Geotechnical Corp., 1964), which consists of Paleozoic intrusives and sediments dipping 30-40° towards the northeast. The APOK signal is very strange indeed, composed of a wave travelling down the well with an apparent vertical velocity of approximately 3.5 km/sec and a horizontally travelling wave with infinite vertical velocity. One possible explanation of this result is again suggested by the dip of the structure (Sax, 1967). The incoming P wave might be refracted by the tilted interface so that the wave front would be a leaking surface wave when it reached the well.

High-resolution frequency-wavenumber spectra are shown for all these data samples in Figures 6, 8, 9b and 10b. These were computed with a signal-to-noise ratio of 2, which seemed to be a good balance between high resolution and excessive distortion. For the WMSO examples, the technique decreased the width of the -3db contour by more than a factor of two for both the cases of noise and signal. The results are more difficult to assess for the vertical array data because of the "whitening" in frequency done by the filters. However, for the noise sample at 0.25 cps, a decrease by a factor of two in the width of the -3db contour can again be seen.

A marked disadvantage and a difficulty still to be solved in the application of this technique is illustrated in Figure 10b. The high-resolution technique, when applied to short samples of data, can produce spurious peaks in the frequency-wavenumber spectra. These are due to the limited smoothing done when computing spectra from short samples of data. Figure 10b shows several of these peaks. This is regarded as an unrecoverable distortion and in a certain sense, an inevitable result of using a high-gain procedure.

References

Baldwin, R., 1964, A re-evaluation of S/N improvement for CPO using local noise: Special Report No. 5, Project VT/4053, Contract No. AF33(657)-12747: Texas Instruments, Inc., Dallas, Texas.

Burg, J.P., 1967, Maximum entropy spectral analysis: Paper presented at the 37th Meeting of the Society of Exploration Geophysicists, Oklahoma City, Oklahoma.

Geotechnical Corp., 1964, Semi-annual Report No. 6, Project VT/1139 (Deep-hole seismometer), Contract No. AF33(600)-43369: The Geotechnical Corporation, Garland, Texas.

Haney, W.P., 1967, Research on high-resolution frequency wavenumber spectra: Special Scientific Report No. 2, Project VT/6707, Contract No. AF-33(657) 16678: Texas Instruments, Inc., Dallas Texas.

Lintz, P.R., 1968, An analysis of a technique for the generation of high-resolution wavenumber spectra: Seismic Data Laboratory Report (in press), Project VT/6702, Contract No. F33657-67-c-1313: Earth Sciences Division, Teledyne, Inc., Alexandria, Virginia.

McCowan, D.W., 1967, Finite Fourier Transform theory and its application to the computation of correlations, convolutions, and spectra: Seismic Data Laboratory Report No. 168 (Revised), Project VT/6702, Contract F33657-67-c-1313: Earth Sciences, Teledyne, Inc., Alexandria, Virginia.

Rizvi, S.A., et al., 1967, Analysis of K-line wavenumber spectra from three WMO noise samples: Advanced Array Research Special Report No. 2, Project VR/7701, Contract No. F33657-67-c-0708-P001: Texas Instruments, Inc., Dallas, Texas.

Sax, R.L., 1967, Frequency-wavenumber analysis of signals and noise recorded at the vertical array at Apache, Oklahoma: Seismic Data Laboratory Report No. 196, Project VT/6702, Contract No. F33675-67-c-1313: Earth Sciences, Teledyne, Inc., Alexandria, Virginia.

Spieker, L.J., et al., 1961, Seismometer array and data processing system: Final Report Phase I, Project No. VT/977, Contract No. AF-33(600)-41840: Texas Instruments, Inc., Dallas, Texas.

D. Best Linear Unbiased Estimation for Multivariate Stationary Processes

Many problems in the area of applied time series analysis can be formulated and solved by extending and generalizing well known techniques from the classical theory of the multivariate linear hypothesis. The analogies between some of the physical models expressed in terms of signals propagating across arrays and the usual analysis of variance models involving various kinds of effects are striking, particularly when it can be assumed that the multivariate stochastic process in question is weakly stationary. In the stationary case, simplicity in exposition as well as economy in computation result from performing the analysis in the frequency domain using the properties of the Fourier transform.

As an example of a simple estimation problem suppose that a multivariate stochastic process $\{Y_j(t),\ j=1,2,\ldots,n,\ -\infty < t < \infty\}$ consists of a signal which is identical for each j

and a weakly stationary multivariate noise process. More specifically we assume that

$$Y_j(t) = s(t) + n_j(t) \qquad j=1,2,\ldots,n \qquad -\infty < t < \infty$$

In this model s(t) is regarded as a fixed unknown signal with $n_j(t)$ a weakly stationary zero mean multivariate noise process with a correlation function given by

$$R_{jk}(t-t') = En_j(t)n_k(t') = \int_{-\infty}^{\infty} e^{i\omega(t-t')}\,\sigma_{jk}(\omega)\,\frac{d\omega}{2\pi}$$

where we assume that $\sigma_{jk}(\omega)$ is the cross spectral density matrix of the noise process. The notation is simplified if we use continuous parameter processes and the results apply equally well to the discrete parameter sampled data version. By a best linear unbiased estimate (BLUE) of the signal, say $\hat{s}(t)$, is meant the unbiased linearly filtered version of the data ($E\hat{s}(t) = s(t)$) which has the smallest variance ($E(\hat{s}(t) - s(t))^2 = \text{min.}$). This problem is analogous to estimating the mean of a set of correlated random variables and has been previously considered by Kelly and Levin (5), and Capon, Greenfield, and Kolker (1). The inherent advantage of this model over the Wiener approach (for example see Papoulis, (8) is that it is not necessary to know in advance the functional form the signal in order to minimize the mean square error or variance of the signal estimate.

The general solution for BLUE estimators given by $H(\omega) = (X^* \sum^{-1} X)^{-1} X^* \sum^{-1}(\omega)$ requires that the spectral matrix of the noise be known; although this is seldom the case, good estimates for $\sum$ can sometimes be obtained by using a sample of noise when

the regression coefficients $\beta_j(t)$ are not present. In the next section we show how the general linear model through an appropriate choice for $X_{jk}(t)$ can be specialized to a number of interesting cases occurring in practical applications.

The theoretical results are easily extended to discrete time parameter processes by replacing integrals with summations and the infinite frequency range by $(-\pi<\omega<\pi)$ but in the application to finite time sampled data certain approximations are necessary. We must decide first whether the analysis proceeds more reasonably and economically in the time domain or the frequency domain. We have chosen the frequency domain for several reasons. First, the restrictions imposed by certain signal models must allow for time delays as long as 300 digital points. This means that the time domain analogue of the matrix product $(X^* \Sigma^{-1} X)^{-1}$ becomes extremely large if a 512 point time delay preserving filter is required. Hence, the frequency domain approach becomes much faster as the analysis can be performed separately at each frequency. In addition, it has been noted in Capon, Greenfield, and Kolker, (1) that short filters designed in the time domain are more sensitive to slight stationarity and signal model perturbations. Reference 1 also contains several examples illustrating time and frequency domain computations and concludes that the loss due to using a two sided infinite lag filter rather than the physically realizable filter obtained in the time domain is small.

The approximations used in the examples below are based on the use of the finite Fourier transform and involve replacing the data and filter by aliased versions of the optimum infinite

two-sided Fourier transforms. References 2 and 7 contain excellent material describing the theory and application of the finite Fourier transform. The effects of aliasing are reduced by choosing an appropriate sampling interval in time based on the highest frequency observable in the data. In the two examples given below the signals are limited to the band from 0 to 10 cycles per second (cps) with the major frequency content less than 5 cps. Hence, the data can be sampled with $\Delta t = .05$ seconds yielding an aliasing frequency of 10 cps. The data samples are long with the first being 150 seconds (3,000 pts) and the second 60 seconds (1200 points) so that $-\infty < t < \infty$ is approximately valid. Finally, the accuracy of the various approximations employed can be evaluated from simulated examples similar to those given below.

Example 1

Here we consider the model given by

$$Y_j(t) = s_1(t) + s_2(t-T_j) + n_j(t)$$

$$j = 1,2,\ldots,20$$

This model is equivalent to two interfering signals recorded at the same time.

Figure 11 shows the first five channels of data constructed to conform with the above equation. Two seismic signals and smoothed white noise uncorrelated from channel to channel were added in the same proportions to produce twenty channels. Five of the twenty channels are displayed in Figure 11. The general signal estimation procedure was to compute the matrix product

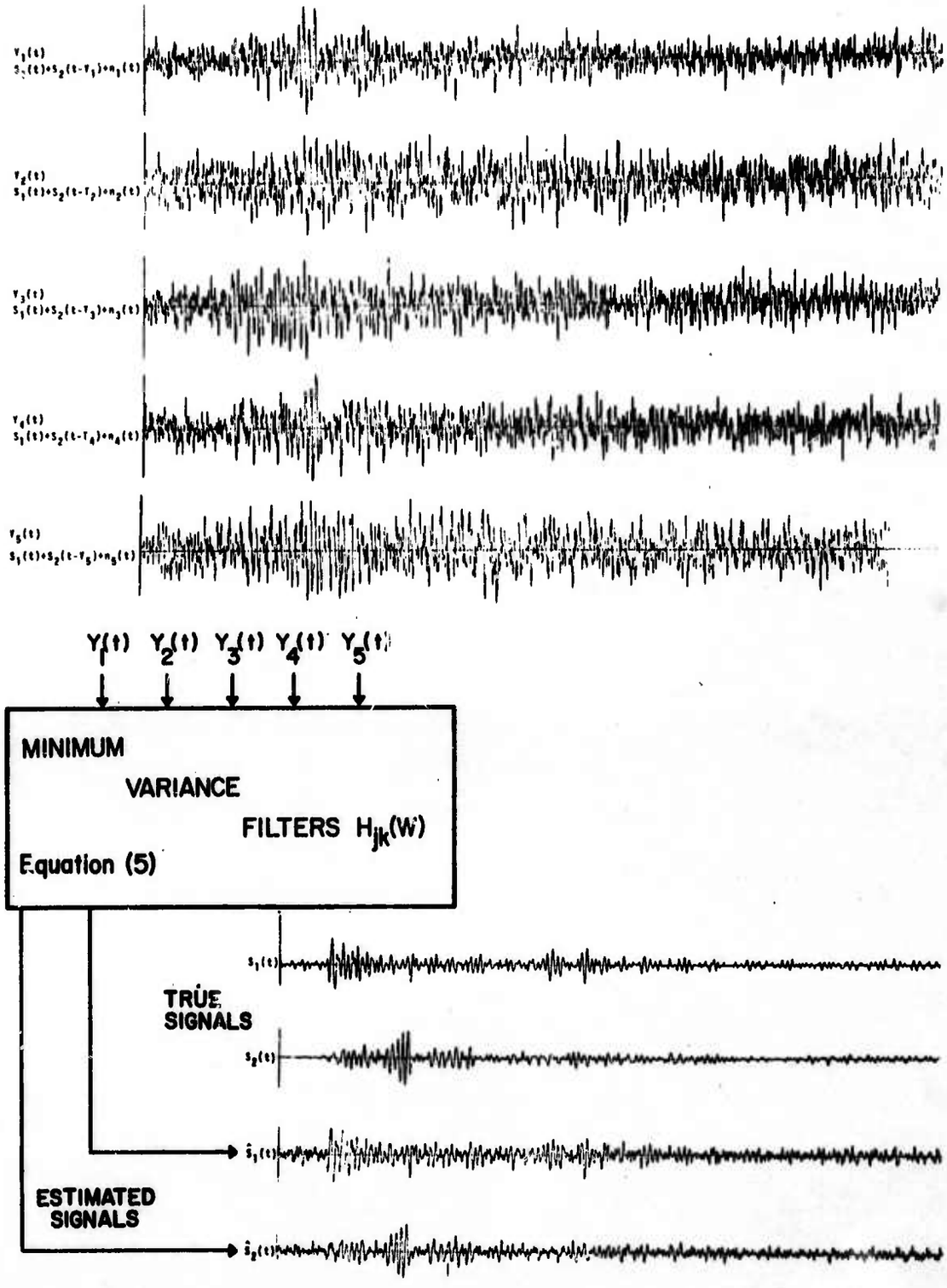

Figure 11 Separation of Two Mixed Signals By Minimum Variance Filters

$(X^*X)^{-1}X^*(\omega)$ at each of 256 frequencies. The singularity at $\omega = 0$ was eliminated by tapering the frequency response functions down to zero at 0 cps. A fast Fourier transform subroutine (see McCowan, 7) applied to the frequency response matrix $H(\omega)$ produced the impulse response functions shown in Figure 12. Note that the net results of the filters are to reinforce and sum the aligned signal $s_1(t)$ while cancelling the second signal $s_2(t)$ which appears at the given time delays. The reverse holds when estimating $s_2(t)$ with the unaligned signal reinforced and the aligned signal cancelled. The signal estimates are formed using a high speed convolution subroutine which calculates a matrix product in the frequency domain and then re-transforms the result to obtain time domain estimates for the regression functions. Note that in the application of the convolution each $Y_j(t)$ is available only for the finite interval T and we assume that $Y_j(t) = 0$ for t & T. The true signals $s_1(t)$ and $s_2(t)$ are displayed along with the estimates $\hat{s}_1(t)$ and $\hat{s}_2(t)$ in Figure 11. The generation of the filters at 256 frequencies or 512 time points for 20 channels took eight minutes of CDC 1604 time with the subsequent convolution requiring thirty minutes. However, by combining the operations in a different order the total running time has been reduced to eight minutes.

Example 2

As an example of a more complicated model consider the multivariate process recorded on a vertical array shown in Figure 13. Each level or channel conforms artificially to the model,

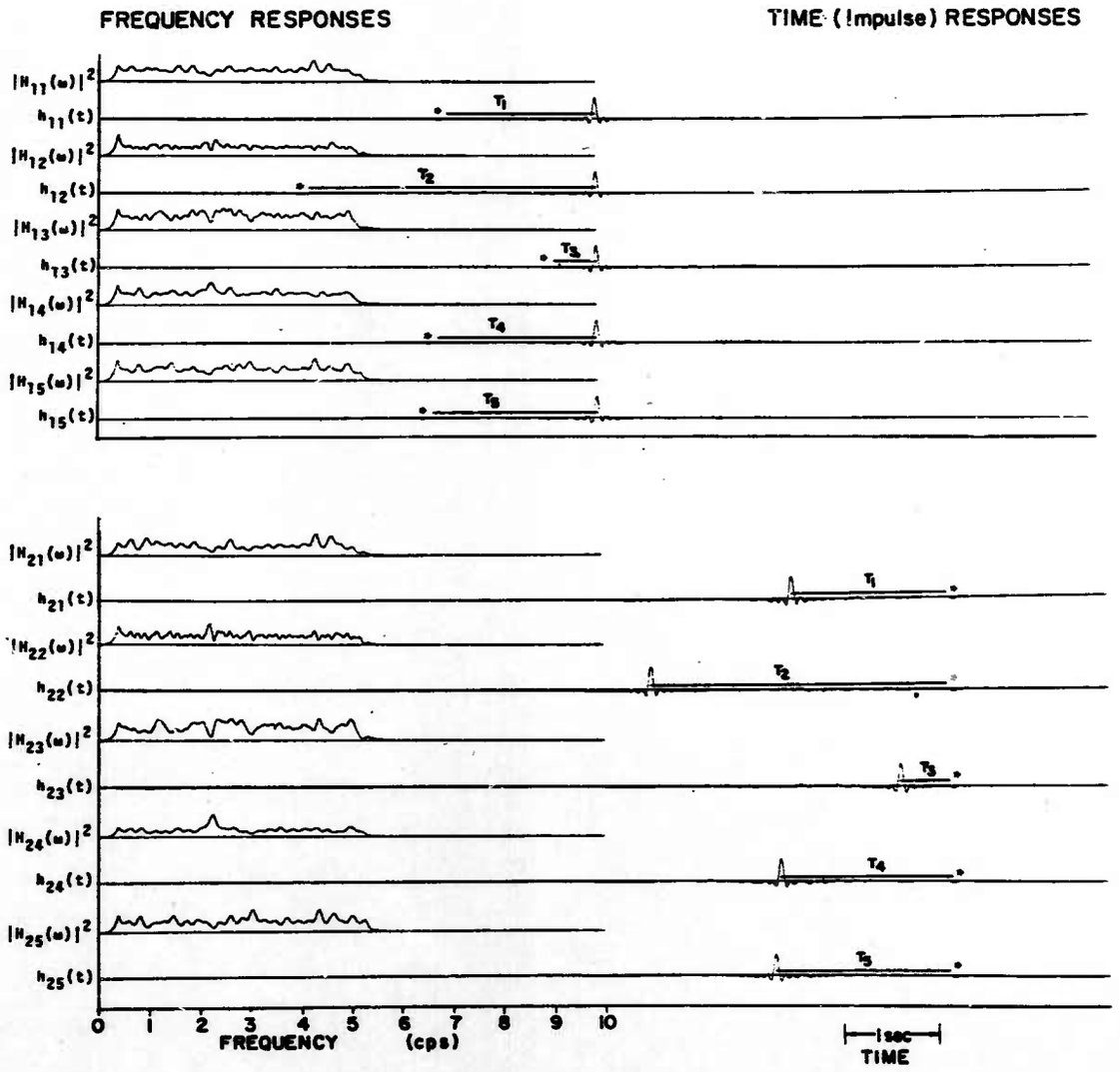

Figure 12 Multiple Channel, Minimum Variance Filters For Estimating Two Mixed Signals

$$Y_j(t) = \beta_1(t) + \sum_{m=2}^{4} \int_{-\infty}^{\infty} X_{jm}(t-u) \quad \beta_m(u)\ du + n_j(t)$$

$$(j = 1,\ldots,5)$$

The data representing a teleseismic signal and several Rayleigh modes, was generated by adding noise and the known functions $\beta_j(t)$ in Figure 13 to the data using the transfer functions $X_{jk}(t)$. The real valued frequency responses ($X_{jk}(f)$m $f = \omega/2\ \pi$ cps) are shown in Figure 14 for the range 0 to 2 cps. The response functions were low pass filtered with a cutoff at 2 cps: hence, there is no significant frequency response above that value. The optimum filters in this case were 200 points or 10 seconds long and were computed by evaluating the matrix product $(X^*X)^{-1}X^*(\omega)$ at 200 frequencies. (The fast Fourier transform was not used here so the number of data points is not a power of two). The resulting matrix of filter coefficients was convolved with a multivariate process to generate the estimates shown in Figure 13. Comparison of these estimated regression functions with the true regression functions indicates that the procedure again produces reasonable estimates.

References

1. Capon, J., Greenfield, R.J., and Kolker, R.J., 1967, Multi-dimensional Maximum-Likelihood Processing of a Large Aperture Seismic Array, Proceedings of the IEEE, Vol. 55, #2.

2. Cooley, J.W., P.A.W. Lewis and P.D. Welch, 1967, The Fast Fourier Transform and its Applications, IBM Research Paper, RC-1743.

3. Goodman, N.R., 1963, Statistical Analysis Based on a Certain Multivariate Complex Gaussian Distribution, Ann. Math. Statist., 34, 152-177.

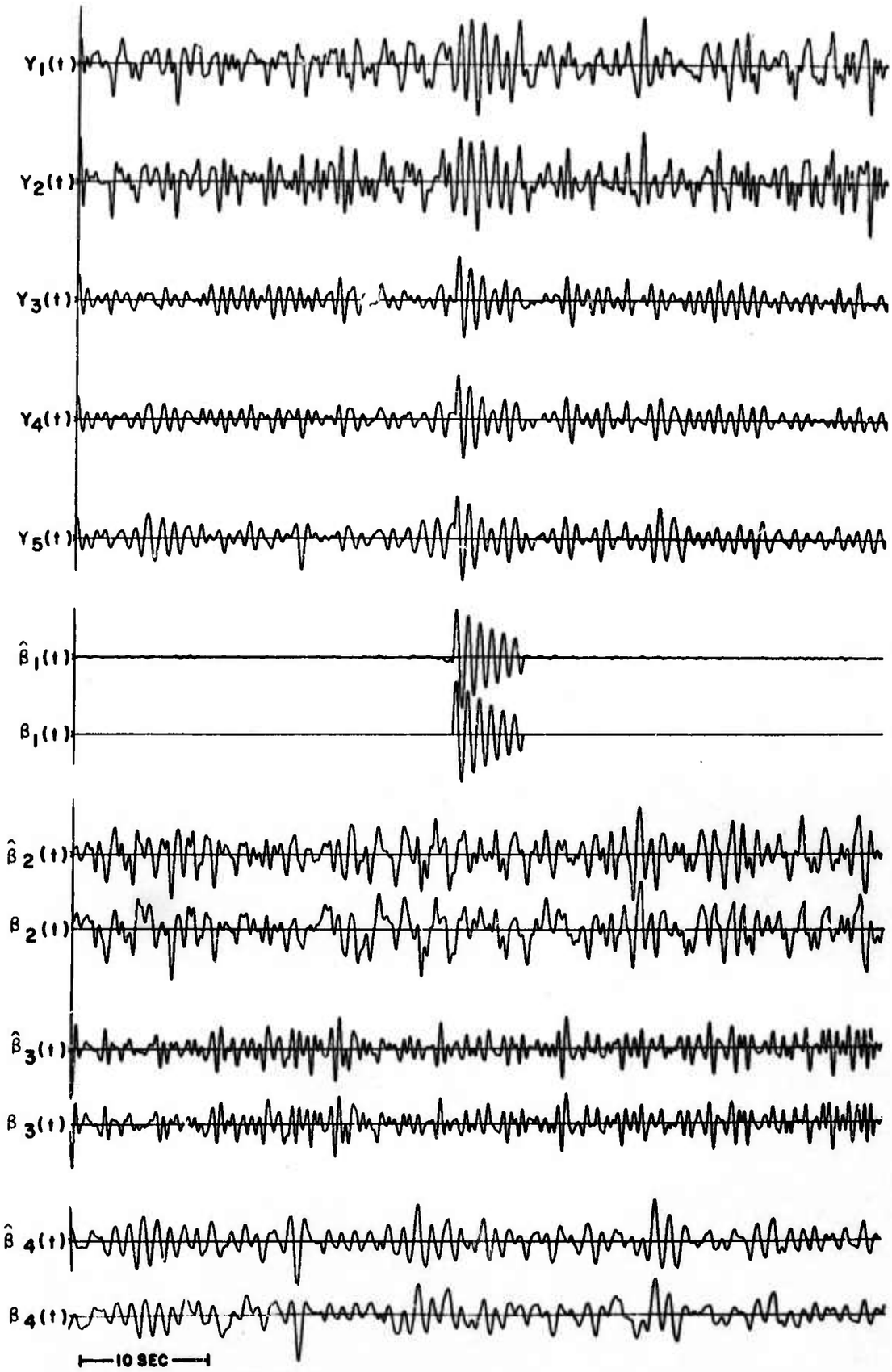

Figure 13 - Basic Data and Estimates Compared With True Values

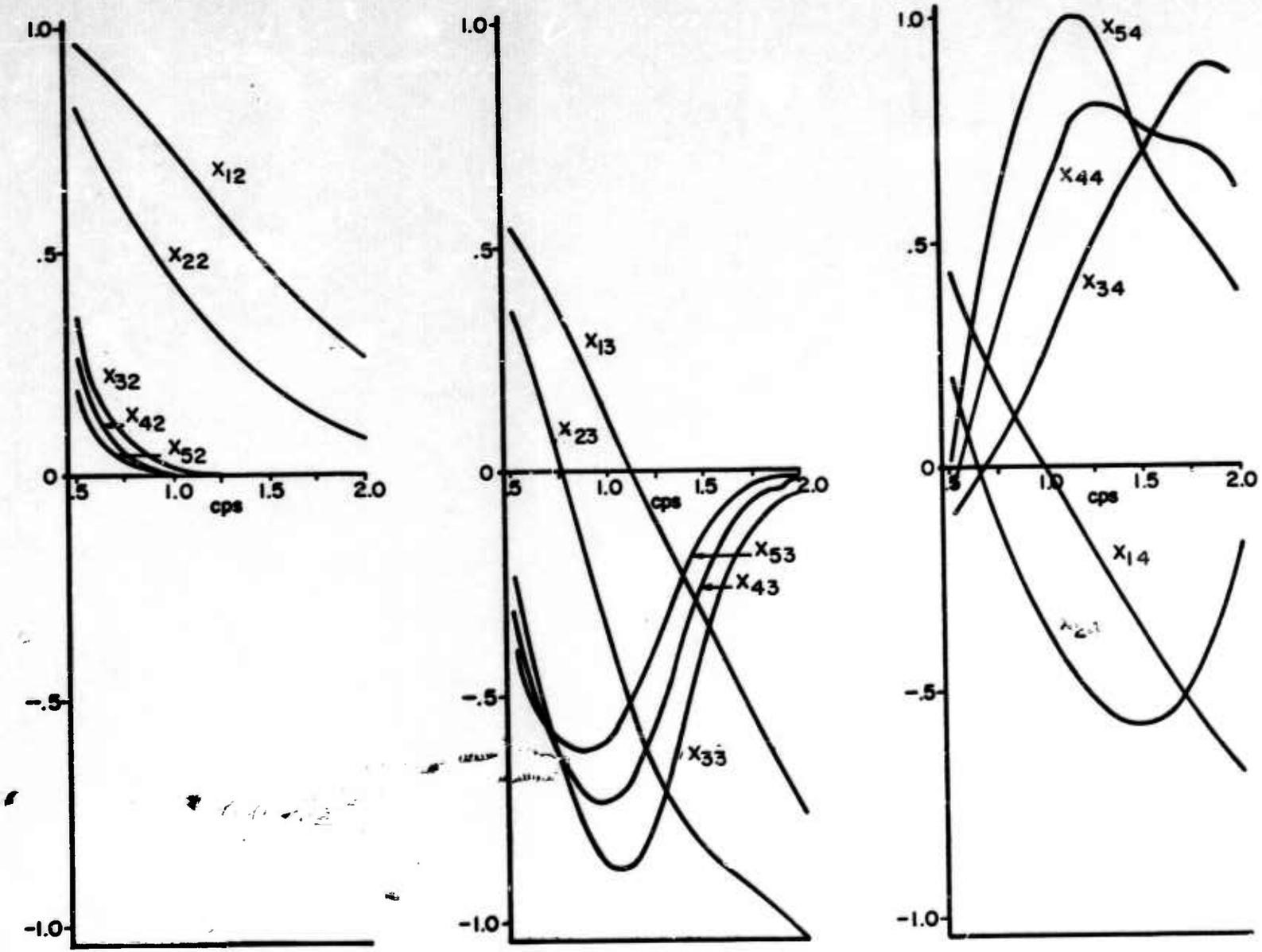

Figure 14 - Matrix of Observations $X_{jk}(f)$, $\omega=2\pi f$, f=cps

4. Grenander, U. and Rosenblatt, M., 1957, Statistical Analysis of Stationary Time Series, John Wiley.

5. Kelly, E.J., Jr., and Levin, M.J., 1964, Signal Parameter Estimation for Seismometer Arrays, MIT Lincoln Lab., Tech. Report 339.

6. Kullback, S., 1959, Information Theory and Statistics, John Wiley.

7. McCowan, D.W., 1966, Finite Fourier Transform Theory and its Application to the Computation of Correlations, Convolutions and Spectra, Seismic Data Laboratory Report No. 168 (Revised), Teledyne, Inc., Alexandria, Virginia.

8. Papoulis, A. 1965, Probability, Random Variables, and Stochastic Processes, McGraw-Hill.

9. Parzen, E., 1961, An Approach to Time Series Analysis, Ann. Math. Statist., 34, 951-989.

10. Rosenblatt, M., 1956, Some Regression Problems in Time Series Analysis, Proceedings of the Third Berkeley Symp. on Math. Statist., and Probability, Univ. of California Press, Berkeley.

E. Design and Evaluation of Certain Multichannel Filters

The first phase of the SDL multichannel filter project, namely, the design and evaluation of certain multichannel filters has been concluded. Experimental results obtained by applying the various multichannel filters to actual seismic array data are used to reach certain conclusions about the performance of the various multichannel filters.

The practical computation of many of these filter operators relies heavily on the fast Fourier transform algorithm of Cooley and Tukey, without which many of the calculations would not even be possible. An earlier report (McCowan, 1966) dealt

with the transform method and its associated techniques and the present report can be regarded as a logical development of the ideas presented there.

The standard of comparison used to grade multichannel filter performance is the unbeamsteered sum of the data channels. This was chosen instead of the beamsteered or phased sum simply as a matter of convenience. Straight summation is itself an optimum processor when the signals are aligned and the noise is uncorrelated. Any departures from this model either in signal misalignment of noise correlation, will, of course, detract from the theoretically best performance, which is the square root of the number of sensors increase in signal to noise (S/N) ratio improvement. This is where the multichannel filter is applicable; the design equations are a theoretical statement of these departures in signal and noise models. Filters satisfying these equations should provide an increase in S/N ratio improvement over the otherwise optimum processor, the straight sum.

The data used in the experimental part of this report were from an Aleutian earthquake recorded by ten sensors in the D1 subarray of the Montana LASA. Ten sensors were used instead of the original twenty-five available in the D1 subarray to reduce the computation time and to simplify the procedure of tabulating results. This particular set was selected to provide a reasonably geometric array with good element separation. Calibrations were computed in the usual manner and all traces were corrected to true ground motion.

For some parts of the study, the traces were prefiltered with the "SDL" bandpass filter. This filter is a phaseless four-pole Butterworth recursive filter. It was chosen to provide a balance between excessive signal distortion at one end and good noise reduction at the other.

As in previous SDL data-processing reports, the definition of signal amplitude will be one-half the maximum peak-to-trough amplitude occurring in the first three cycles of the P phase. Noise is defined as the root-mean-square amplitude measured over some specified interval. The S/N ratio is the quotient of these two quantities. Frequently results will be expressed in db for which the usual expression will be used, $20 \log_{10}(\text{RATIO})$. When the quantities to be expressed in terms of db have the dimensions of power, this definition has been changed to $10 \log_{10}(\text{RATIO})$ in order to preserve the proper amplitude ratio.

The results of this study are presented in Table 2 which lists the actual improvement in S/N ratio over the unprefiltered straight sum for the various multichannel filters. Simply bandpass filtering the sum gets 15 db improvement in S/N ratio at practically no expense of computer time, so the real comparison is with this reference level. The amplitude of the noise was computed for the measured noise multichannel filter outputs over an interval of 200 seconds, including the fitting interval and 100 seconds outside the fitting interval. The maximum-likelihood noise amplitude was also computed over an interval of 200 seconds, but this time including the fitting interval and 50 seconds outside it. Therefore, these noise levels represent an average of the rms noise amplitude inside fitting interval and outside it. This problem does not, of course, arise with the straight sums and theoretical isotropic processor outputs.

TABLE 2

MULTICHANNEL FILTER REPORT

S/N Ratio Improvement

Filter	Data	Signal Model	db Improvement
Unphased Sum	UBPF	--	0
Theoretical MCF	UBPF	10 km/sec	7
Theoretical MCF	UBPF	Infinite	4.8
Maximum Likelihood	UBPF	--	15
Measured-Noise MCF	UBPF	10 km/sec	3
Measured-Noise MCF	UBPF	Infinite	-6
Unphased Sum	BPF	--	15
Theoretical MCF	BPF	10 km/sec	16.4
Theoretical MCF	BPF	Infinite	16.1
Maximum Likelihood	BPF	--	17
Measured-Noise MCF	BPF	10 km/sec	10.3
Measured-Noise MCF	BPF	Infinite	5

We can make several comparisons in this table. The first concerns the amount of frequency filtering that is done. The illusory gains from the maximum-likelihood filter operating on un-prefiltered noise come about because the least-squares equation does not constrain the filter to do otherwise. Many degrees of freedom in the filter weights are misused doing what could be done with just elementary processing, i.e., bandpass filtering. Apparently all but 2 db of the original 15 db can be accounted for by bandpass filtering. On the other hand, the design equation for the measured-noise multichannel filter specifies as a desired signal spectrum one of the noise spectra. Therefore, some frequency filtering is expected. The design equation for the theoretical multichannel filter assumes a flat spectrum for the desired signal output. However, the filter which satisfies this equation is only the optimum filter in the least-squares sense, so we should expect some, but not much, frequency filtering. This is demonstrated in the table. In summary, the maximum likelihood multichannel filter is the worst regarding frequency filtering and the theoretical multichannel filter is the best.

Secondly, in both cases, the theoretical and the measured noise filters designed with a disc signal model ($V \geq 10$ km/sec) performed better than the infinite-velocity filters. This fact is true in general and is a direct result of not beamsteering the array. However, other results discussed below suggest that this gain occurs only in a frequency band higher than the signal band. For the prefiltered theoretical multichannel filter, designed on noise where this energy has been removed, this difference only amounts to 0.3 db.

Finally, as regards isotropic processor multichannel filters, the theoretical processor is always better than the measured-noise processor. This is a strange and completely unexpected result, probably arising from the fact that the noise seems to overlap the signal model in k space. For a measured-noise multichannel filter this represents a contradiction of specification in the least-squares design equations which could lead again to a misuse of the degrees of freedom available in the filter weights. The theoretical multichannel filter is not computed from actual data and hence is not affected.

The conclusions listed below are based upon results obtained from processing only one event. In view of this they should be accepted with due caution.

1. Designing multichannel filters on un-prefiltered noise gives an illusory S/N ratio improvement which is not attained with similar multichannel filters designed on prefiltered noise.

2. Isotropic processors can be effectively applied to unbeamsteered arrays, provided a finite velocity signal model is used.

3. Measured-noise isotropic processors are not effective in improving S/N ratio when the noise has large high-velocity components. In this case the theoretical multichannel filter is the superior processor.

4. With the exception of the maximum-likelihood filter evaluated for performance within its fitting interval, only the theoretical multichannel filter showed a gain over the

prefiltered straight sum. That gain was slightly more than 1 db, which is not regarded as significant.

5. One drawback of the maximum-likelihood filter is its unnecessarily complex response in k-space. It does not appear that modifying the constraint will cure this.

References

Bendat, J.S., and Piersol, A.G., 1966, Measurement and Analysis of Random Data, John Wiley and Sons, New York.

Blackman, R.B., and Tukey, J.W., 1959, Measurement of Power Spectra, Dover Publications, Inc., New York.

Burg, J.P., 1964, Three Dimensional Filtering with An Array of Seismometers: Geophysics, Vol. 29, No. 5, pp 693-713.

Capon, J., and Greenfield, R.J., 1965, Asympototically Optimum Multidimensional Filtering for Sampled-Data Processing of Seismic Arrays: Tech. Note 1965-67, MIT Lincoln Laboratory, Lexington, Mass.

Claerbout, J.F., 1964, Detection of P-Waves from Weak Sources at Great Distances: Geophysics, Vol. 29, pp. 197-210.

Cooley, J.W., and Tukey, J.W., 1965, An Algorithm for the Machine Calculation of Complex Fourier Series: Math. of Comp., Vol. 19, pp. 297-301.

Cooley, J.W., et al, 1967, The Fast Fourier Transform Algorithm Adaptation and Its Application: Research Paper RC 1743, IBM Research Center, Yorktown Heights, New York.

Flinn, E.A., et al., 1966, Two Examples of Maximum-Likelihood Filtering of LASA Seismograms: Seismic Data Laboratory Report No. 148, Earth Sciences Division, Teledyne, Inc., Alexandria, Virginia.

Flinn, E.A., and Claerbout, J.F., 1965, Some Topics in Digital Filtering Theory and Application: Research Dept. Memo., Earth Sciences Division, Teledyne, Inc. Alexandria, Virginia.

Kelley, E.J., and Levin, M.J., 1964, Signal Parameter Estimation for Seismometer Arrays: Tech. Report 339, MIT Lincoln Laboratory, Lexington, Mass.

Levinson, N., 1949, The Wiener RMS Error Criterion in Filter Design and Prediction: Appendix B in: Extrapolation, Interpolation, and Smoothing of Stationary Time Series, by Norbert Wiener, MIT Press, Cambridge.

McCowan, D.W., 1966, Finite Fourier Transform Theory and Its Application to the Computation of Correlations, Convolutions, and Spectra: SDL Report No. 168 (Revised) 1967, Earth Sciences Division, Teledyne, Inc., Alexandria, Va.

Spieker, V.J., et al., 1961, Seismometer Array and Data Processing System: Final Report. Phase I, AFTAC Project No. VT/077, Contract AF 33(600) 41840, Texas Instruments, Dallas, Texas.

F. Digital Computer Programs for the Design and Evaluation of Multichannel Filters

The following is a list of program write-ups for the multichannel filter program set written under the multichannel filter project at the SDL. All of these programs were verified using write-ups which are now as free from errors as possible. This set of programs should provide a reasonably complete capability to analyze signals and noise, design multichannel filters to enhance signals and suppress noise, evaluate the performance of these filters, and prepare the punched paper tape which inputs the multichannel filters into the Texas Instruments Digital converter.

An alphabetical list of the programs described in SDL Report 210 along with corresponding COOP identification numbers is shown below:

G621	COLYTUKY	M221	MCFONPT
G627	COHERENCY	G630	MULTICOH
G638	CONFIL	G631	PARTLCOH
G624	FKSPTRUM	G636	PLOTFK
G632	HEFALUMP	G628	PREDICT
G640	ISOFIL	G635	SPECAVE
G639	LSTCHNCE	G625	TWX
Z124	MAXLIK	G629	VFKSPTRUM
M220	MCFONPT		

G. Response of Several Vertical Array Processors

The SDL frequency-wavenumber analysis program VFKSPTRM (1966) was used to calculate the response of several simple processors for vertical arrays. The impulse responses of the filters as applied to each channel were subjected to frequency-wavenumber analysis. This implied an equal and simultaneous impulsive input to each channel.

Each processor involves a beamed sum of P-waves based on normal moveout times for vertical compressional waves. The multichannel deghoster and fan filter are followed by other operations designed to remove signal distortion or improve the dead-band response of the processor. The multichannel deghoster estimates the signal waveform at the surface without regard to correlated background noise. The fan filter (1967) ideally passes waves between a specified pass-band of limiting vertical phase velocities and rejects energy outside of the band.

We examined several vertical array geometries. These are specified by uphole times based on the arrival of the upgoing vertical compressional wave at each instrument in the array subtracted from the arrival time at the surface. A vertical phase velocity of 6 km/sec was used for the f-k analysis.

Table 3 correlates the array geometry, type of processor and figure number from the original report. Table 4 illustrates the symbols used for the f-k spectral maps shown in Figures 15, 16, 17, 18, and 19.

Comparing Figure 15 and Figure 17 we see that an 18% increase in the length of the vertical array makes only slight improvement in the array response. An array with maximum uphole time of .55 sec with 6 instruments provides an adequate response in the signal band with the power to discriminate body waves at frequencies above .7 cps.

Figures 16, 18, and 19 show the array response for equally spaced instruments placed in the lower 2/3 of the well. The apparent resolving power is inadequate between 1.0 and 1.3 cps for all of the processors analyzed. The fan filter appears to have the desired pass-band response with better dead-band rejection than the beamed sum and multichannel deghoster.

Several of the simplest vertical array processors were evaluated by means of frequency-wavenumber spectral analysis. The processors analyzed were beamed sum, multichannel deghost, and the fan filter. Adequate responses were obtained in the specified signal pass-band for all of the processors. Considerable differences between the processors were observed in

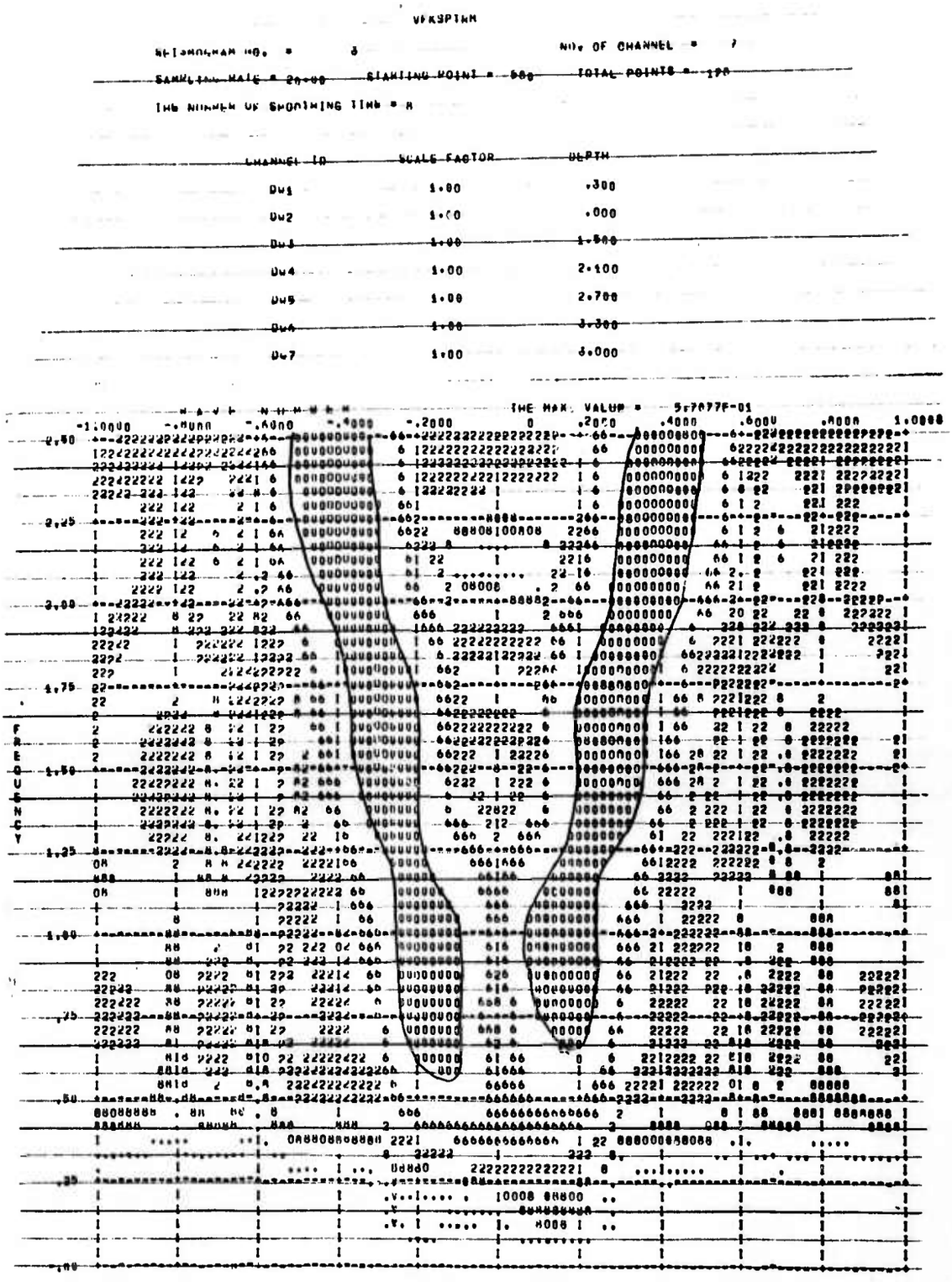

Figure 15. Beamed Sum

Figure 16. Beamed Sum

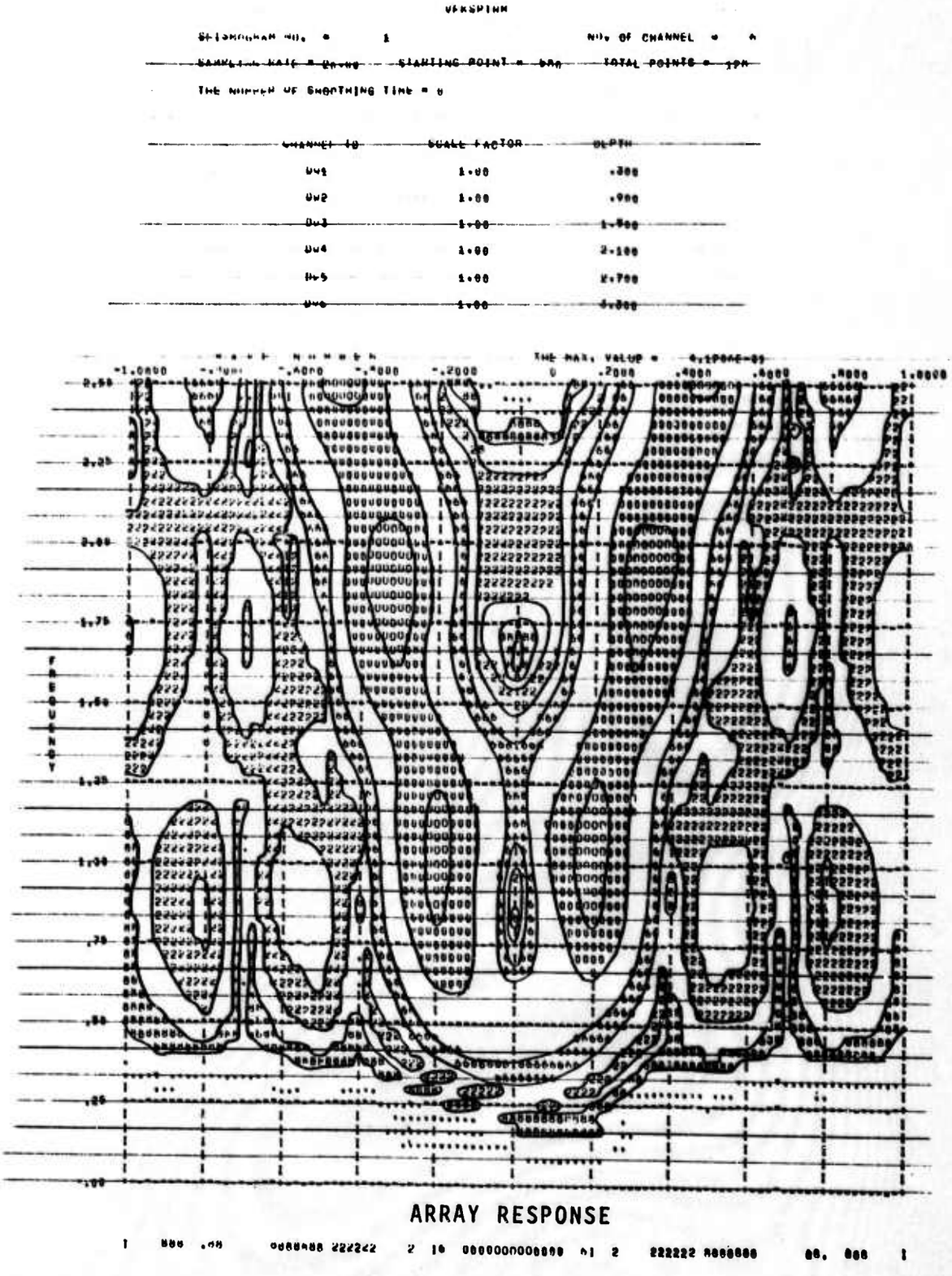

Figure 17. Beamed Sum

VFKSPTRM

SEISMOGRAM NO. = 2 NO. OF CHANNEL = 6

SAMPLING RATE = 20.00 STARTING POINT = 980 TOTAL POINTS = 128

THE NUMBER OF SMOOTHING TIME = 0

CHANNEL ID	SCALE FACTOR	DEPTH
Dw1	1.00	.900
Dw2	1.00	1.500
Dw3	1.00	2.100
Dw4	1.00	2.700
Dw5	1.00	3.300
Dw6	1.00	3.900

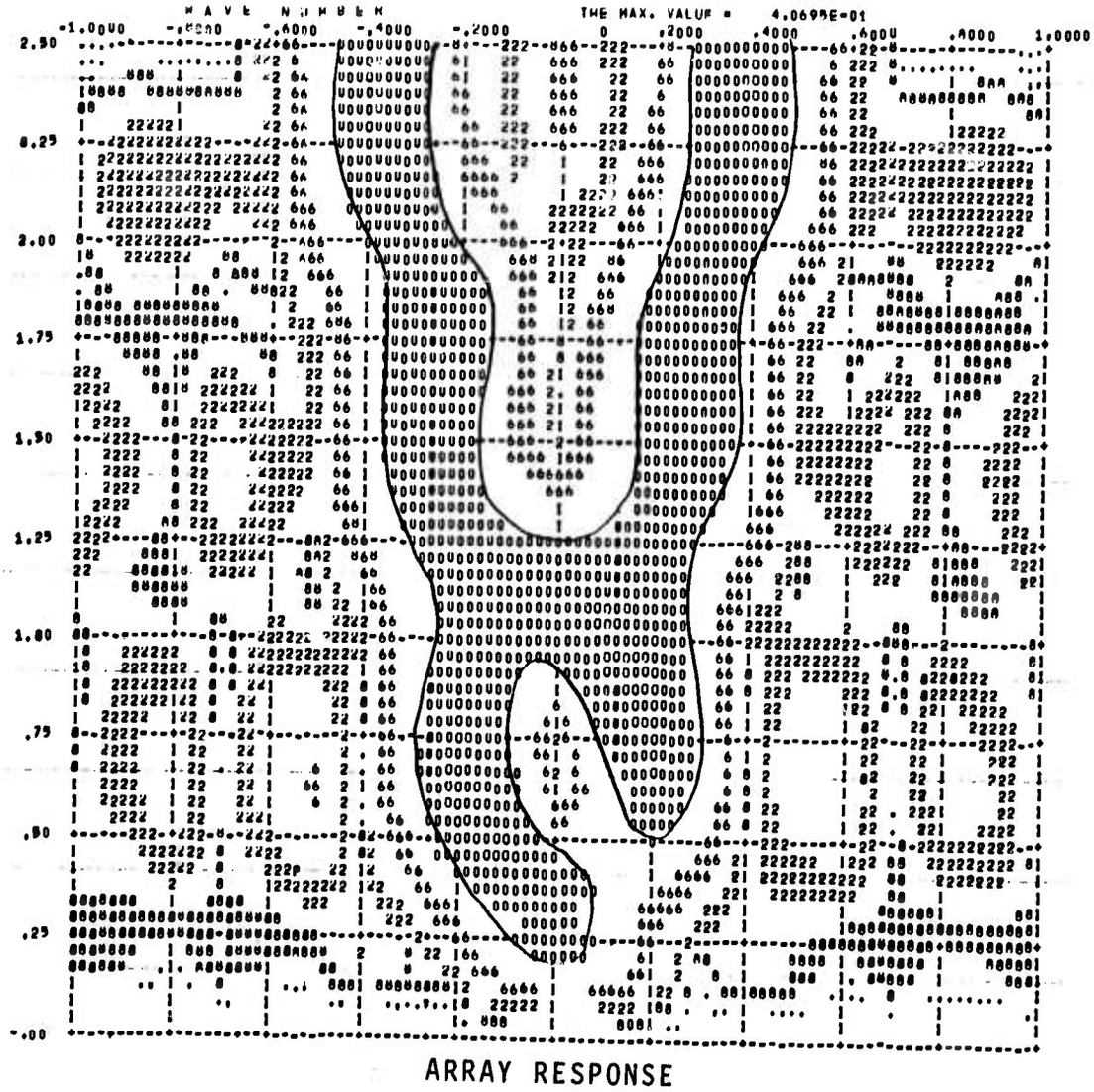

Figure 18. MCdeG

VFKSPTRM

SEISMOGRAM NO. = 1 NO. OF CHANNEL = 7

SAMPLING RATE = 20.00 STARTING POINT = 400 TOTAL POINTS = 100

THE NUMBER OF SMOOTHING TIME = 0

CHANNEL ID	SCALE FACTOR	DEPTH	UP HOLE TIME FOR 6 GEOPHONES
Dw1	1.00	.300	.05
Dw2	1.00	.900	.15
Dw3	1.00	1.500	.25
Dw4	1.00	2.100	.35
Dw5	1.00	2.700	.45
Dw6	1.00	3.300	.55
Dw7	1.00	3.900	.65

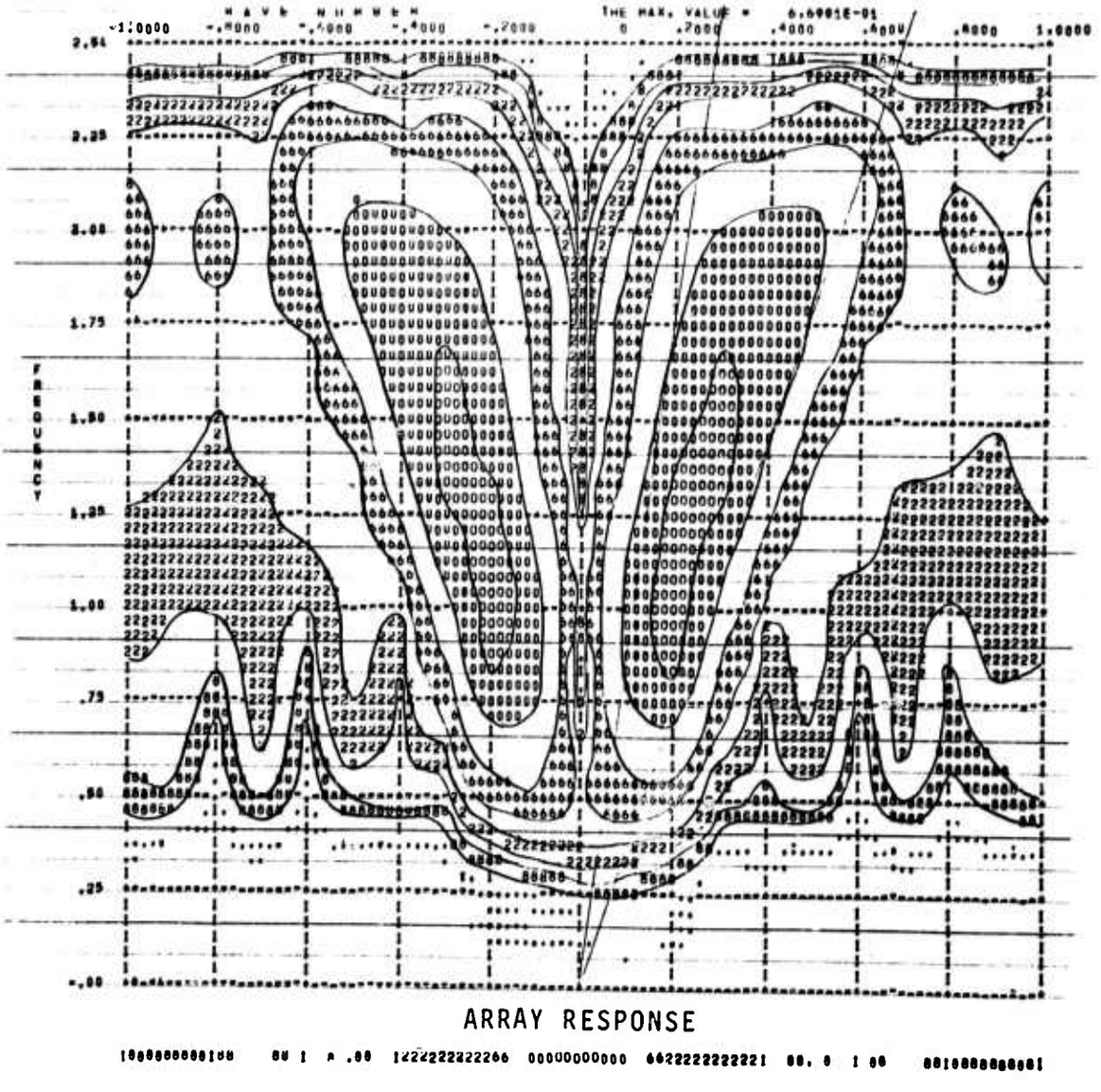

ARRAY RESPONSE

Figure 19. Fan Filter

TABLE 3

Fig. No.	Processor	No. of Channels	Uphole times (sec.)	Frequency Bandpass (cps)	Velocity Bandpass (km/sec)
1	Beamed sum	7	.05,.15,.25,.35,.45,.55,.65	All Pass	0
2	Beamed sum	7	.05,.15,.25,.35,.45,.55,.65	.4 - 3.0	0
3	Beamed sum	7	.00,.15,.25,.35,.45,.55,.65	All Pass	0
4	Beamed sum	6	.15,.25,.35,.45,.55,.65	All Pass	0
5	Beamed sum	6	.05,.15,.25,.35,.45,.55	All Pass	0
6	Beamed sum	6	.05,.15,.25,.35,.45,.55	0.4 - 3.0	0
7	MCdeG	6	.05,.15,.25,.35,.45,.55	All Pass	0
8	MCdeG	6	.15,.25,.35,.45,.55,.65	All Pass	0
9	MCdeG	6	.05,.15,.25,.35,.45,.55	0.4 - 3.0	0
10	Fan Filter	6	.05,.15,.25,.35,.45,.55	All Pass	3.0-9.0
11	Fan Filter	6	.05,.15,.25,.35,.45,.55	0.4 - 3.0	3.0-9.0
12	Fan Filter	7	.05,.15,.25,.35,.45,.55,.65	0.4 - 3.0	3.0-9.0
13	Fan Filter	6	.15,.25,.35,.45,.55,.65	All Pass	3.0-9.0
14	Fan Filter	6	.05,.15,.25,.35,.45,.55	All Pass	4.5-7.5

TABLE 4

Symbols For the F-K Spectral Mapping

DB	Symbol
0-1	0
1.001 - 3	0
6-9	6
12-15	2
18-21	8
24-27	.

the dead-band, especially at low wavenumbers corresponding to surface wave components in the noise. The best dead-band response was obtained for the fan filter using a spacing with uphole time between instruments of .1 seconds from the top to the bottom of the well.

References

McCowan, D.W., Finite Fourier Transform Theory and its Application to the Computation of Convolutions, Correlations, and Spectra, Seismic Data Laboratory Report No. 168 (Revised), Teledyne, Inc., Alexandria, Virginia.

Treitel, S., Shanks, J.L., Frasier, C.W., Some Aspects of Fan Filtering, Geophysics, Vol. 32, n. 5, 1967.

H. Hyperfine Beamsteering Using a Signal Crosscorrelation Technique

By beamsteering we mean shifting different array channels in time and forming a sum. The beam output is frequently also referred to as the "phased sum" or "delay-and-sum output" (Chiburis and Hartenberger, 1966). The interchannel time shifts consist of those calculated from an assumed signal propagation velocity across the array and an assumed direction of signal arrival as well as shifts which are intended to compensate for variation in transmission path phase characteristics between elements of the array, i.e., travel time anomalies. For LASA, these time adjustments have been observed to depend on the signal azimuth and phase velocity, that is, on the signal source region (Chiburis, 1966).

In beamsteering the LASA subarrays, only signal velocity is used; the intra-subarray travel time anomalies are negligible.

However, when beaming subarray beams the travel time anomalies are significant: reduction in signal loss of approximately 5 db has been observed when the travel time anomalies are applied (Chiburis, 1966).

However, signal loss of approximately 1 db has been observed in beaming LASA subarrays (Chiburis and Hartenberger, 1966), and another 2-3 db of signal loss occurs when beaming the subarray beams. There appear to be two major contributing factors to the latter signal loss which are variation in signal waveform across LASA and small errors in the travel time anomalies applied.

In this report we describe a method which should reduce signal losses due to the second of these causes. This method can be fully automated, provided that the signal arrival time is known and the signal/noise ratio is not too small -- further work will be required to establish the threshold.

The first step is to measure the differences in signal arrival time which remain in the subarray beams after they have been time-shifted by both signal velocity and azimuth and the travel-time anomalies. Given the signal arrival time and knowledge of the signal duration based on prior experience, two methods for computing the signal arrival time differences suggest themselves.

In the first method we choose one of the N subarray beams as a reference channel. Compute the N-1 crosscorrelations of the other subarray beams with the reference channel, using a properly chosen time window around the signal arrival time (at this point the necessity for already having the signals almost

lined up is apparent). Measure the lag at which each of these N-1 crosscorrelations peak. Assume that these lags give the inter-channel time shifts remaining to be applied.

In the second method we compute the entire correlation matrix of the N subarray beams, using a properly chosen time window around the signal arrival time. Measure the lag for each of the ½N (n-1) crosscorrelations peak. Assume that these represent differences between inter-channel time shifts remaining to be applied. There are thus ½N(N-1) observations from which we can determine the N time shifts by least squares, having ½N(N-3) degrees of freedom (which is a lot). Estimate the standard error of each time shift, and do not apply any time shift which is not significantly different from zero. This should avoid the danger of nonsense results when the signal/noise ratio is small; see the discussion below.

The second method is obviously better than the first since it uses all possible correlations instead of just N of them. Also, the first method can be expected to fail if the reference channel happens to have a small signal or a signal waveform profoundly different from the others (significant variations in waveform have been observed; see, e.g., Flinn et al., 1966).

The only apparent relative drawback to the second method is computing time; but the difference in computing time between the first and the second method is actually quite small. Consider 21 subarray beams and a time window 150 points long. Then the first method requires the computation

of twenty lags of each of twenty 150-point correlations, which requires a small fraction of a second on the CDC 1604-B. The second method requires the computation of 231 correlation functions (our library routine calculates the auto-correlations as well as the cross-correlations), and the solution of 210 condition equations in 20 variables. Forming the correlation matrix should require approximately three seconds. It turns out that the solution of the least-squares normal equations for the time shifts can be written down explicitly without any matrix multiplication or inversion. Thus the computing time is approximately three seconds, which is not excessive.

Notice that the problem is not quite complete as we have stated it so far: a constraint is necessary. We choose one channel as a reference channel and constrain its time shift to be zero; i.e., we compute all the shifts relative to a reference channel (we emphasize again that the accuracy of the least-squares computed shifts in no way depends on the reference channel's having a good signal, as does the first method).

The results of this study are presented in the second part of Table 5 and in Figures 20 through 25. Figure 20 shows the signals from the three events used for computing the cross-correlation matrix. All 5 seconds shown were used to compute cross-correlation functions sampled as often as the data (20 samples per second) and out to a maximum time lag of one second. Figures 21, 22, and 23 show the input and output traces for each case; that is, input to and output from the vernier beamsteering program. In these figures, it is possible

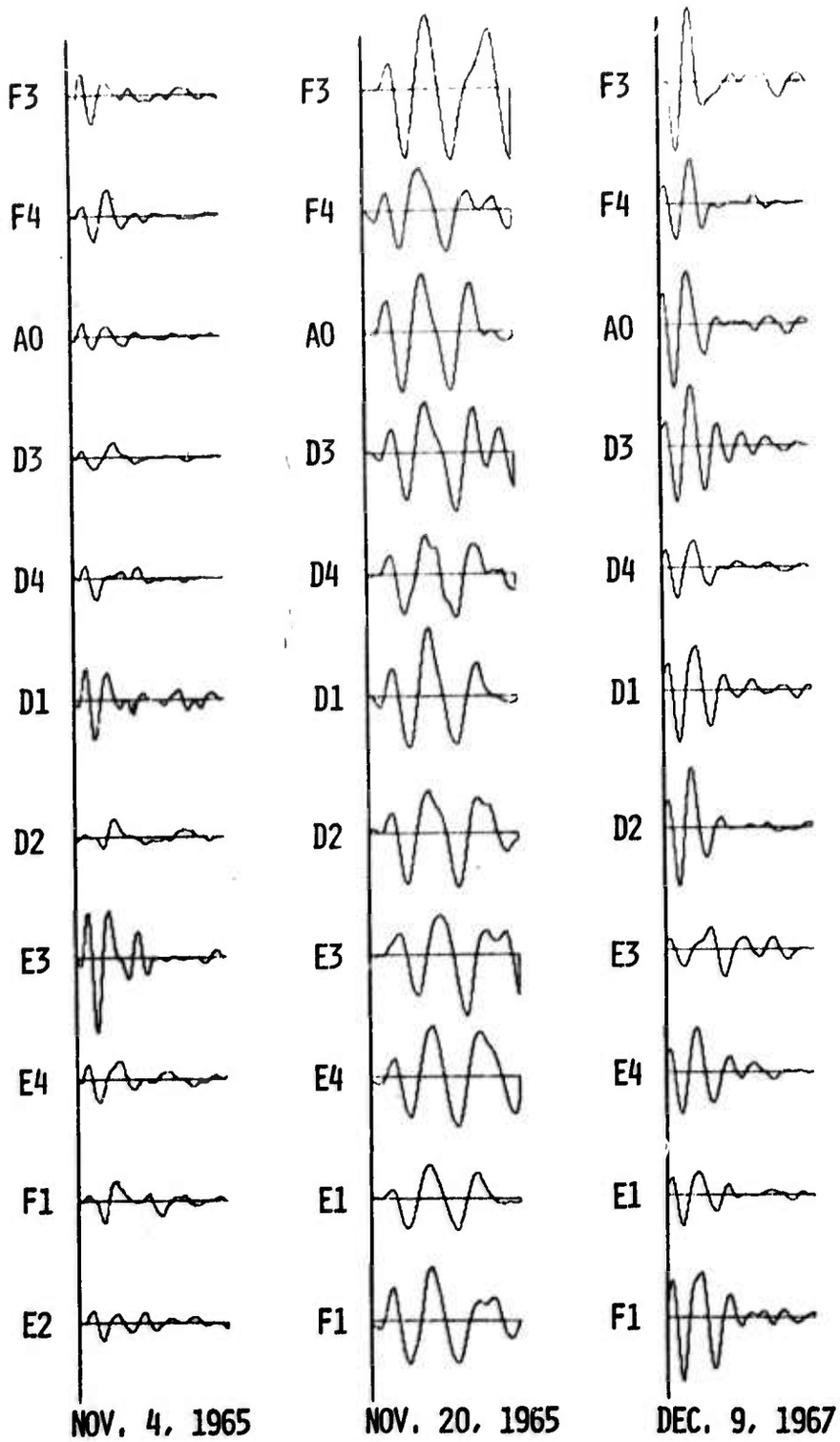

Figure 20. Signals used for computing the cross-correlation functions

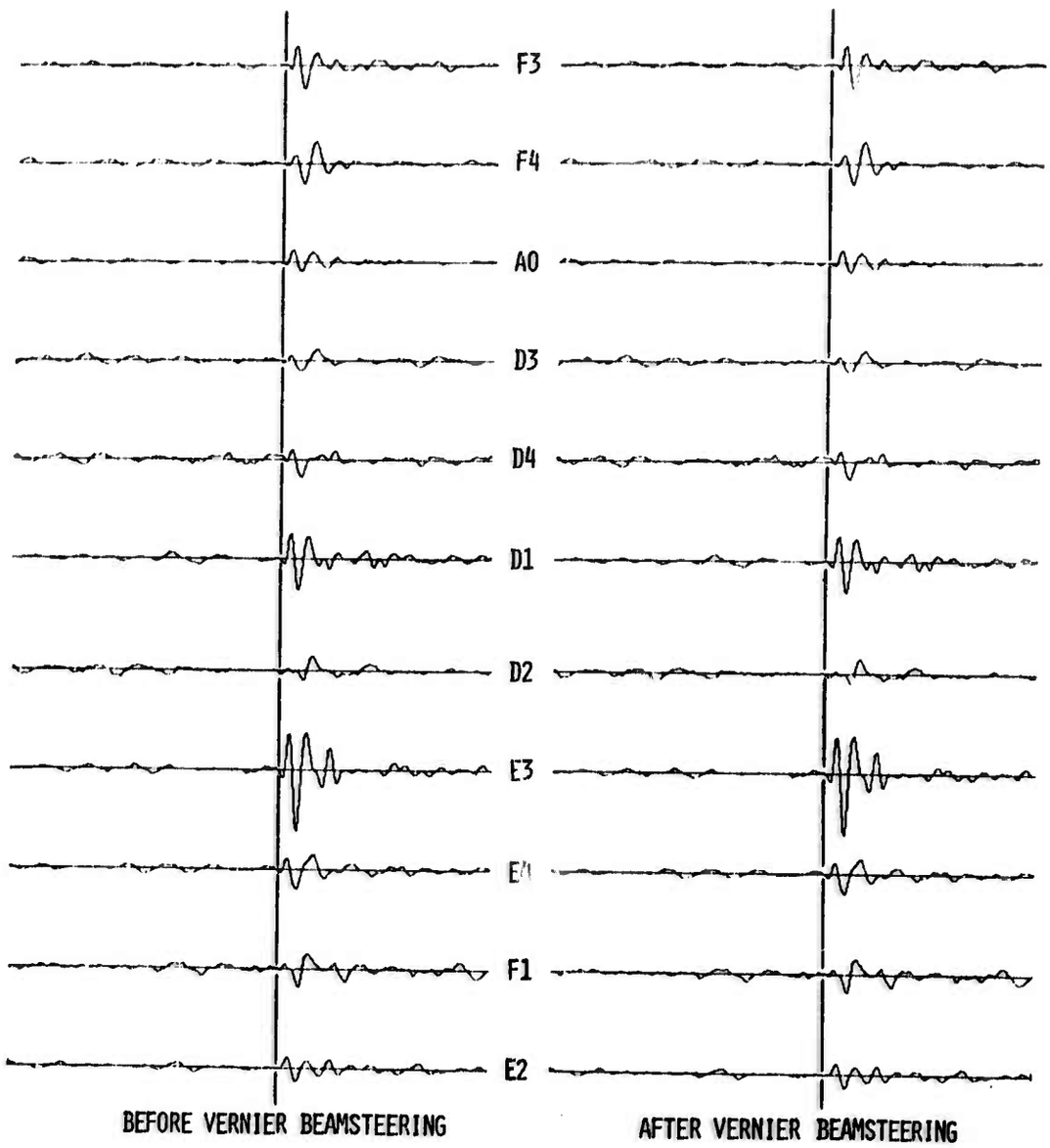

Figure 21. Nov. 4, 1965 event subarray sums

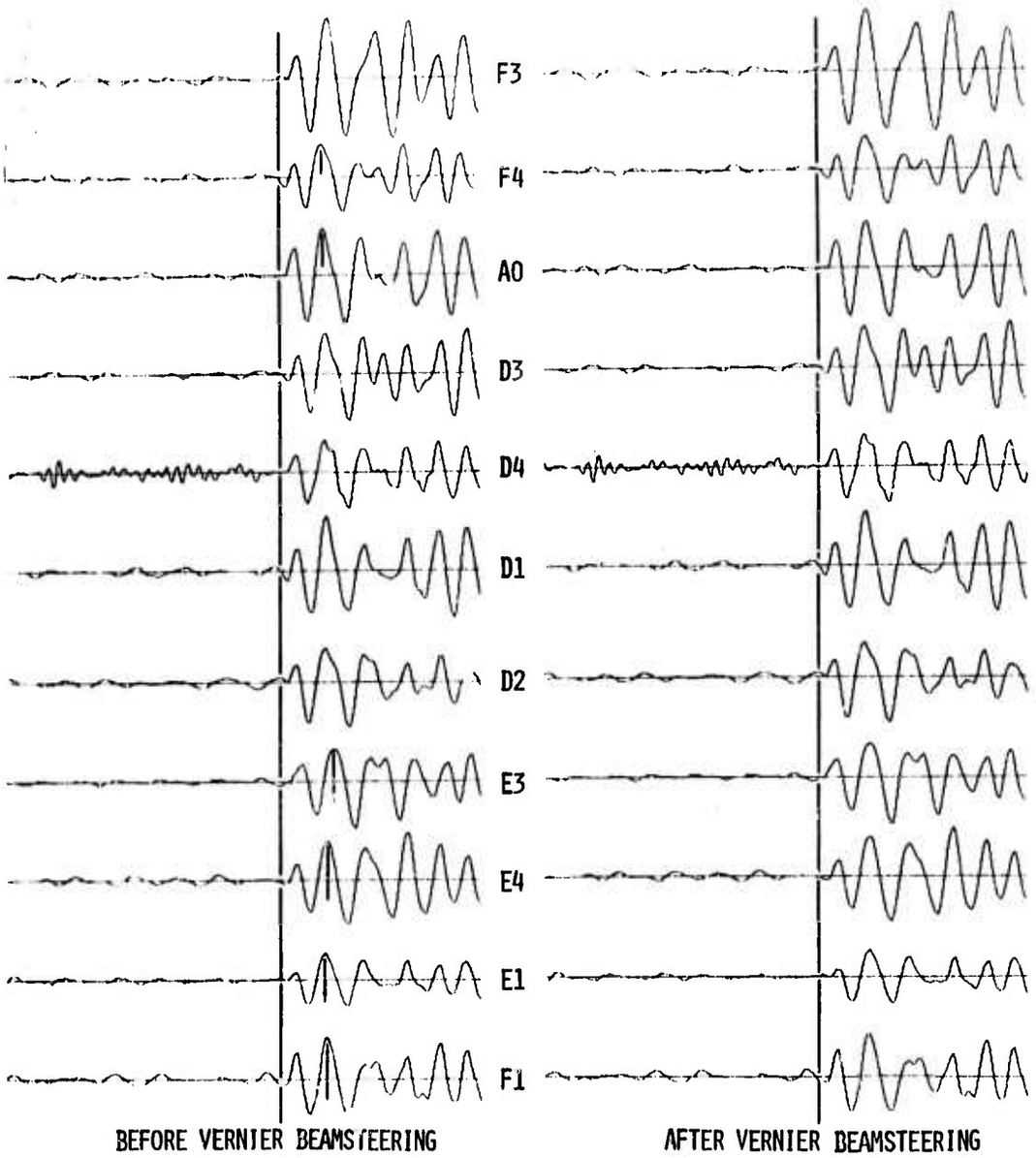

Figure 22. Nov. 20, 1965 event subarray sums

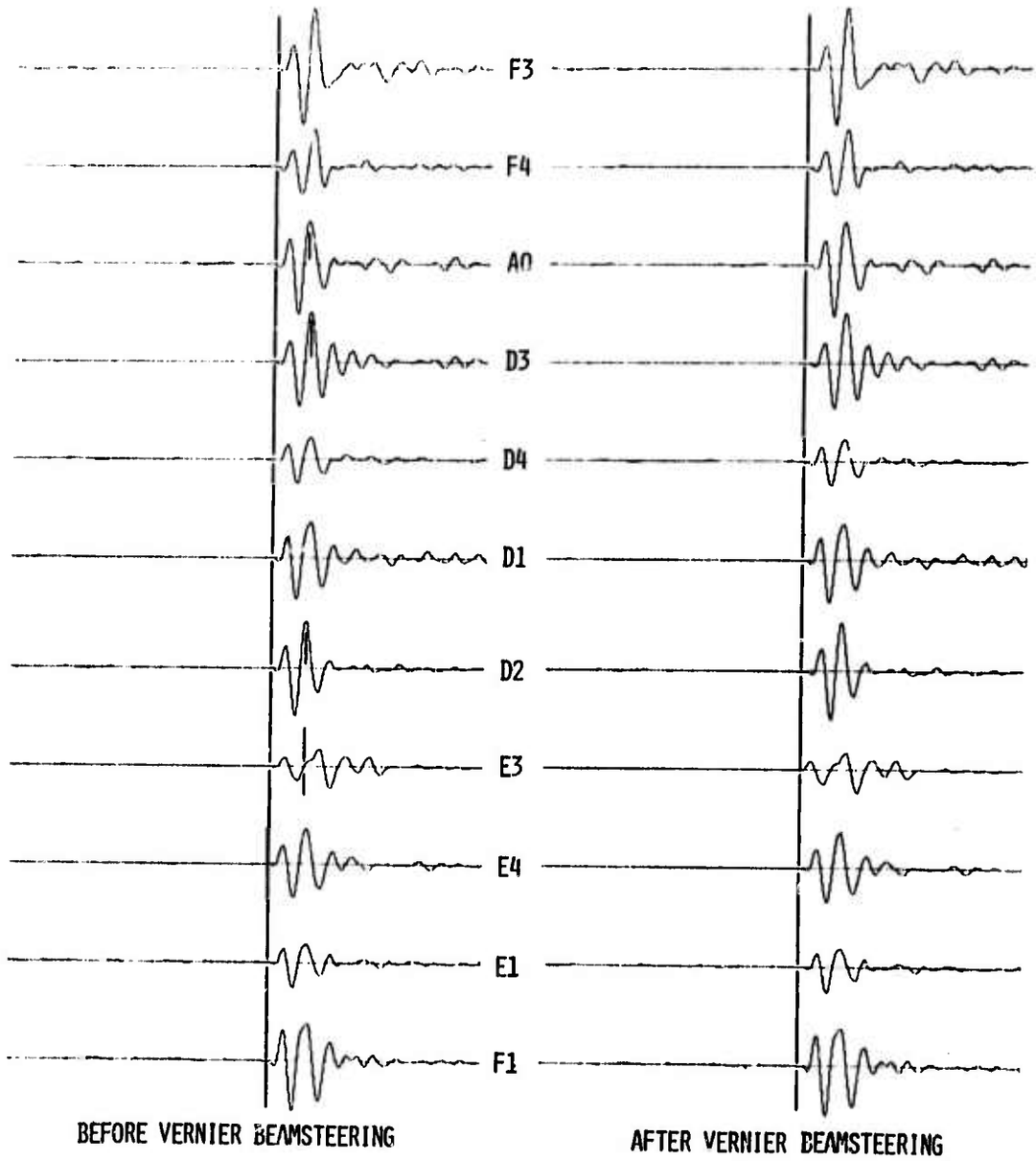

Figure 23. Dec. 9, 1965 event subarray sums

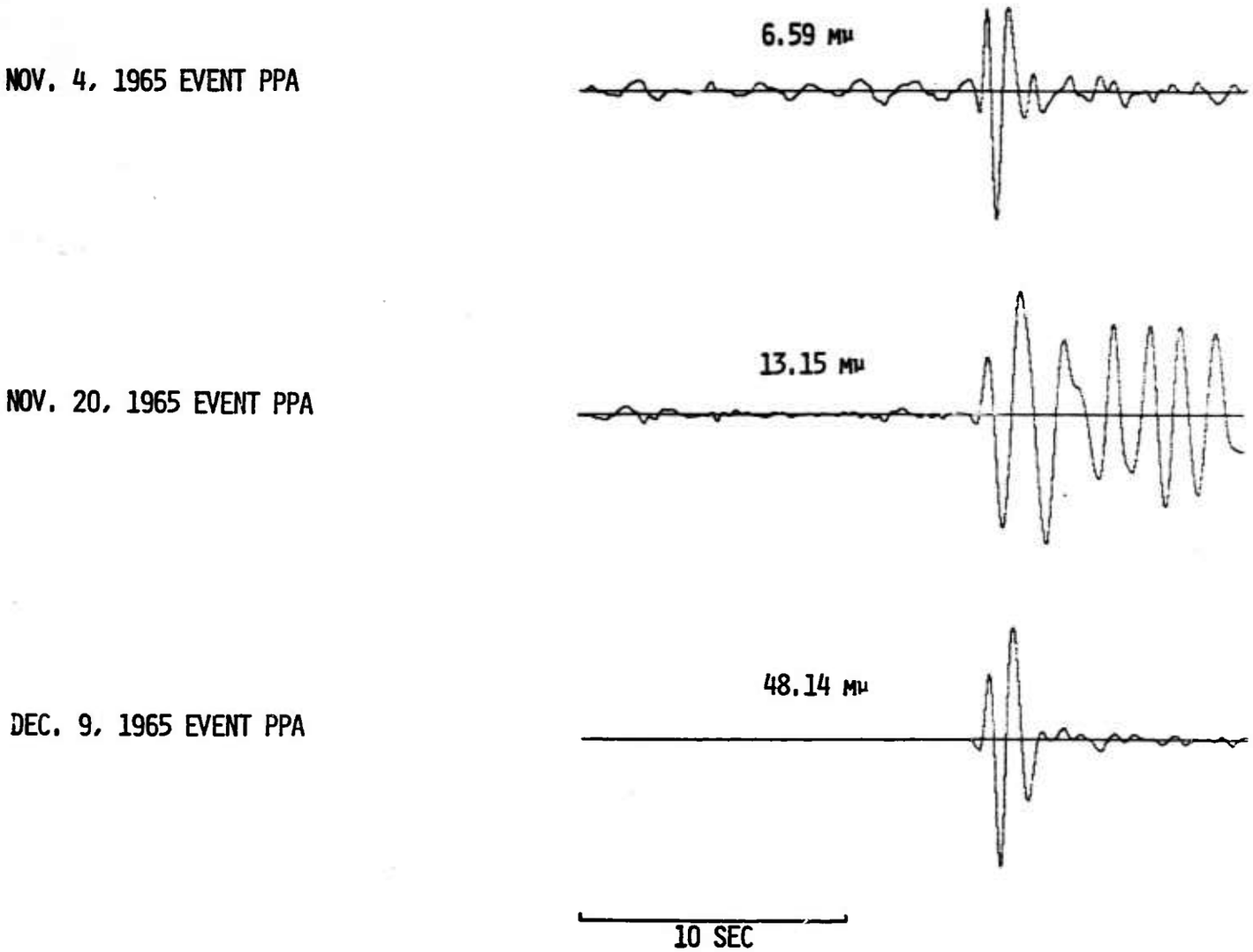

Figure 24. LASA phased sums before vernier beamsterring

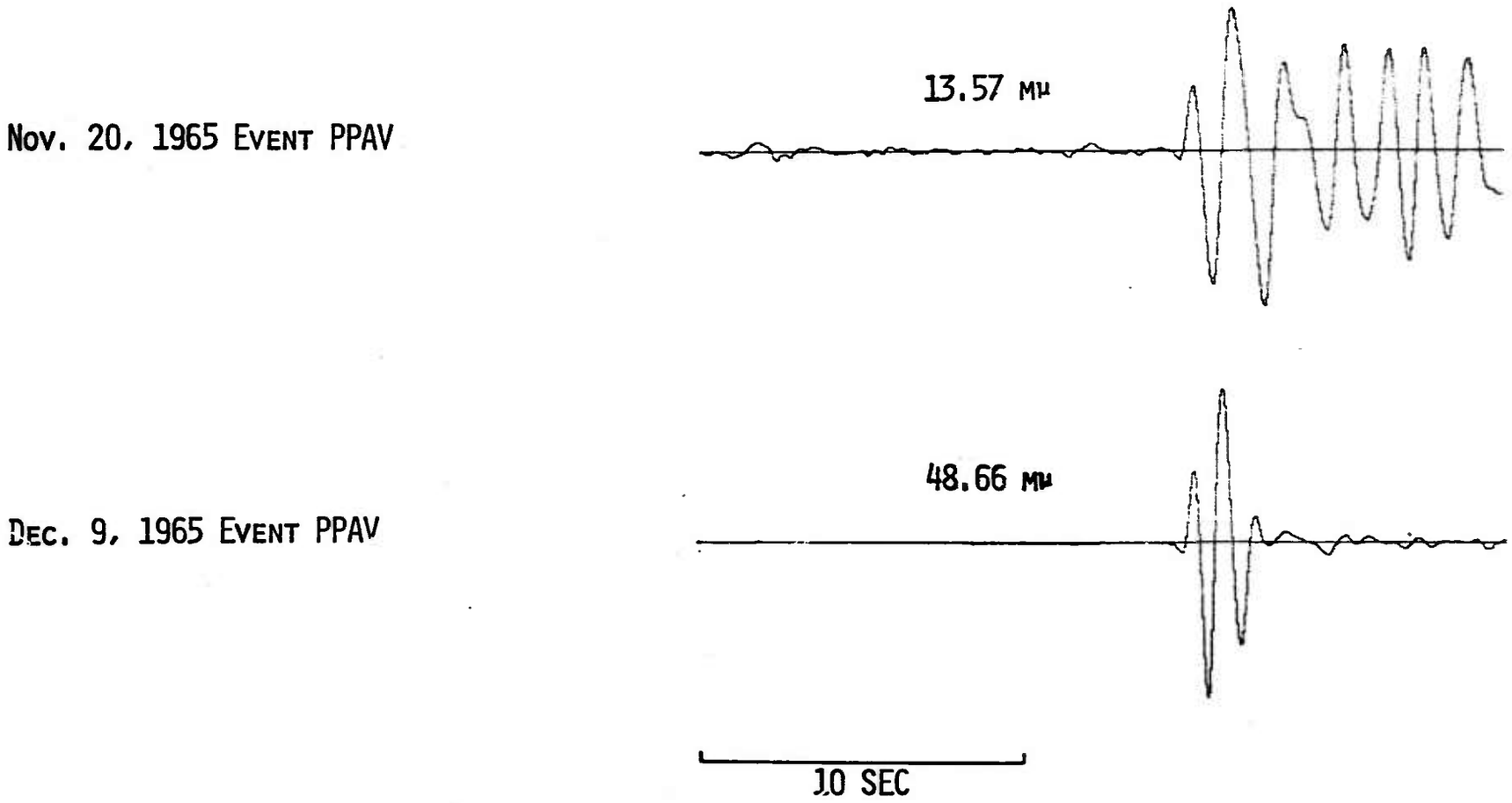

Figure 25. LASA phased sums after vernier beamsteering

TABLE 5

RESULTS

	Nov.4, 1965	Nov.20, 1965	Dec. 9, 1965
PPA Signal (mμ)	6.59	13.15	48.14
PPA Noise rms (mμ)	0.33	0.31	0.34
PPA S/N	19.69	42.61	141.94
PPAV Signal (mμ)	6.59	13.57	48.66
PPAV Noise rms (mμ)	0.33	0.30	0.34
PPAV S/N	19.69	45.76	143.74
Gain (db)	0.0	0.6	0.1
Standard deviation (sec)	.072	.049	.022

to see slight time shifts that were detected and subsequently eliminated by the shifting process. Figures 24 and 25 are the sums before and after processing respectively. The second half of Table 5 lists the numerical results of the study.

The last entry in Table 5 is the standard deviation of the time shifts computed as described above. All of the estimated time shifts for the event were within 2.6 standard deviations of zero and were therefore eliminated. The PPAV for this event is thus equal to the PPA. However, for two other events, six and four time shifts respectively were larger than 2.6 standard deviations. Application of these shifts produces the differences in the input and output for these events. At no time did we have to eliminate a time shift that was greater than half a second.

The standard deviation itself is a good measure of how well the method works. The first event had the lowest signal-to-noise ratio on the PPA trace and the largest standard deviation. The large standard deviation occurs both because of the dissimilarity between the signals from this event and the larger proportionate noise level. On the other hand, another event had the highest signal-to-noise ratio and the lowest standard deviation but did not exhibit the largest gain from the vernier beamsteering procedure. It appears that the anomalies for this event were more accurate than those for the last event. This is supported by the lower number of non-zero shifts.

These results, though small (0.6 and 0.1 db respectively) are nevertheless considered significant. They are corrections to a refined and very accurate process, the phase summation of LASA data using travel time anomalies. Therefore we should expect them to be small. However what makes them important is that they result from eliminating one more cause of signal degredation in phased summation. If one half a db can be saved by vernier beamsteering only 11 subarray outputs, perhaps a full db can be saved by processing all 21. We have demonstrated here a method which resulted (in one case) in reducing by one-half the signal loss actually observed (Chiburis and Hartenberger, 1966).

References

Anderson, T.W., 1958, An Introduction to Multivariate Statistical Analysis, John Wiley and Sons, New York.

Chiburis, E.F., 1966, LASA Travel-time Anomalies for Various Epicentral Regions, SDL Report 159, Seismic Data Laboratory, Alexandria, Virginia.

Chiburis, E.F., and Hartenberger, R.A., 1967, Signal-to-Noise Ratio Improvement by Beamforming LASA Seismograms, SDL Report 173, Seismic Data Laboratory, Alexandria, Virginia.

Flinn, E.A., Hartenberger, R.A. and McCowan, D.W., 1966, Two Examples of Maximum Likelihood Filtering of LASA Seismograms, SDL Report 148, Seismic Data Laboratory, Alexandria, Virginia.

I. Earthquake and Explosion Analysis

Standard statistical summary reports were issued on the Nevada Test Site nuclear events, COMMODORE, SCOTCH, and KNICKERBOCKER. Table 6 summarizes part of the seismic data compiled from these analyses.

Other projects completed included photo albums for two events and travel-time computations for NTS and other sites.

Event Name	Event Date	Medium	Magnitude	No. of Stations Recording SP Signals	LP Signals
COMMODORE	20 May 1967	Tuff	5.68 ± 0.56	21	21
SCOTCH	23 May 1967	Rhyolite	5.51 ± 0.75	21	21
KNICKERBOCKER	26 May 1967	Rhyolite	5.54 ± 0.42	16	16

TABLE 6. Seismic Data from Three Nuclear Explosions

III. SUPPORT AND SERVICE TASKS

A. VELA-Uniform Data Services

As part of the contract work statement, the SDL provided one or more of the following support and service functions for VSC and other VELA participants:

- copies of 16 and 35 mm film.
- playouts of earthquakes and special events.
- copies of composite analog tapes.
- composite analog tapes of special events.
- use of 1604 computer for checking out new programs or running production programs.
- copies of digital programs.
- digitized data in standard formats or special formats for use on computers other than the 1604.
- running SDL production programs, such as power spectral density and array processing on specified data.
- digital x-y plots of power spectra or digitized data.
- signal reproduction booklets.
- space for visiting scientists utilizing SDL facilities to study data and exchange information with SDL personnel.

During this report period, 54 such projects were completed and the 16 organizations receiving these services are listed in Appendix A.

B. Data Library

The data library contains approximately 7400 digitized seismograms, 225 digital computer programs and 293 composite analog magnetic tapes, all available for use by the VELA-Uniform program.

The following additions were made during this period:

1. Digital Seismograms - 400 including
   - data from two explosions
   - one earthquake recorded at various stations
2. LASA Data - 9 tapes
   - there are a total of 1396 digital tapes in the library including 992 field tapes. There is also a master calibration tape which contains the magnification (digital counts per millimicron) of each sensor for every subarray. These magnifications have been computed for all calibration tapes currently in house. As each new calibration is received, it is routinely run through the new program CALIBR and added to the master tape.
3. Digital Programs - 18 including

   TFOASTRO - Information processing - to process an ASTRODATA Seismic Data acquisition system tape and output a digital to analog (DAC) plot tape.

   TFXARII - Data converter for TFO acquisition system tapes. This program makes a standard library seismogram tape from digital tapes in the format of TFO acquisition system tapes.

DEPCATE - Intermediate program of the DEPTHMAG LOCMEV sequence designed to read event data from a DEPTHMAG output tape and prepare an input tape for LOCMEV.

VFSPTRM2 - This program offers an option to project a planar array of seismometer coordinates onto the back-azimuth line before computing the frequency wave-number power spectra. The option of printing out the frequency wave-number power spectra along a velocity line is also available.

LLTOXY - Given the latitude, longitude of one site, the program computes the x and y components in kilometers from this site to other sites of known latitude and longitude within a seismic array.

LOCMEV - This is a modification of LOCATECQ designed to process events from an input tape produced by either the NETMEV or DEPCATE programs. LOCMEV computes the latitude-longitude 95% confidence limits for the input event.

NETMEV - A modification of NETWORK2 designed to produce an output tape containing event locations and selected stations to be processed by the program LOCMEV. The selection of stations for input to LOCMEV are determined by variable criteria designated on the input data deck. LOCMEV computes 95% confidence ellipses for detection of the event by the selected stations.

NORFORM - Processes an Astrodata tape containing short period data, and outputs an unpacked library tape.

TSWITCH - To prepare a binary tape for program LOCATE, containing station directory and travel time and other tables.

TFOSAN - Processes TFO37 data, 20 samples per second, less than 4000 points per channel from a special SDL library tape. This special SDL library tape is made from processing TFO37 data through program TFSARYII, and then through program MERGSEIS. All data to be evaluated by TFOSAN must follow this procedure. The calibrations to be used as data input must first be processed by TFOCAL.

ARRAYPR - Converts an A-D format tape into a UES format library tape and processes the seismograms from an array of seismometers.

MAKTAPE - Program searches digitized data library tapes (packed and unpacked) for requested seismograms and either copies them (on a scratch tape in 1604 Fortran binary format) or writes them in a compatible IBM 7090 format for use by other computer installations.

BMPATRN - To calculate, tabulate, and plot the azimuthal beam patterns for an array steered to enhance a particular velocity or wave number.

LIST80 - Fortran 63 program to list columns 1-80 of program or data cards.

TFOCAL - This program computes magnification levels in counts/microns from the TFO calibration data.

HRVKSPEC - This program computes the high-resolution wavenumber spectrum of seismic linear-array time series data. The spectrum may be calculated with respect to a particular sensor in the array or it may be averaged over all of the sensors in the array.

COMPOSIT - This program copies the header record and section of data from the TFO acquisition system tape onto a composite master tape.

TFSARY3 - This program makes a standard library seismogram tape from digital tapes in the format of TFO acquisition system, composite tapes from the program COMPOSIT.

4. Analog Composite Tapes - 4 including

a. Made by SDL

CHARCOAL
AKTANUM

b. Made by Geotech

GASBUGGY
LANPHER

C. Data Compression

This is a continuing routine operation, and production is maintained at the level needed to meet the requirements of the field operation (LRSM and U.S. Observatories) and the Seismic Data Laboratory. For this period 2218 tapes were compressed.

D. Automated Bulletin Process

November and December 1967 LRSM and Observatory Bulletins were processed during this report period and forwarded to Geotech, a Teledyne Company, for checking and publication.

APPENDIX A

January - March 1968

Organizations Receiving SDL Data Services

Vitro
Geotech
Pennsylvania State University
Colorado School of Mines
International Seismological Centre
IBM
Texas Instruments
General Atronics Corporation
Lincoln Laboratory, MIT
Southwest Center for Advanced Studies
U.S. Coast & Geodetic Survey
Dallas Seismological Observatory
Unitech
Laurence G. Hanscom Field
University of California
Observatorio San Calixto, La Paz, Bolivia

Unclassified
Security Classification

DOCUMENT CONTROL DATA - R&D

(Security classification of title, body of abstract and indexing annotation must be entered when the overall report is classified)

1. ORIGINATING ACTIVITY (Corporate author)

TELEDYNE INDUSTRIES, INC.
ALEXANDRIA, VIRGINIA 22314

2a. REPORT SECURITY CLASSIFICATION

Unclassified

2b GROUP

3 REPORT TITLE

SEISMIC DATA LABORATORY QUARTERLY TECHNICAL SUMMARY REPORT

4 DESCRIPTIVE NOTES (Type of report and inclusive dates)

Quarterly Summary - January - March 1968

5. AUTHOR(S) (Last name, first name, initial)

Hartenberger, Royal A.

6. REPORT DATE	7a. TOTAL NO. OF PAGES	7b. NO. OF REFS
15 April 1968	72	0

8a. CONTRACT OR GRANT NO.	9a. ORIGINATOR'S REPORT NUMBER(S)
F 33657-68-C-0945	
b. PROJECT NO. VELA T/6702	
c. ARPA Order No. 624	9b. OTHER REPORT NO(S) (Any other numbers that may be assigned this report)
d. ARPA Program Code No. 8F10	Technical Summary Report No. 19

10. AVAILABILITY/LIMITATION NOTICES

This document is subject to special export controls and each transmittal to foreign governments or foreign nationals may be made only with prior approval of Chief, AFTAC.

11. SUPPLEMENTARY NOTES	12. SPONSORING MILITARY ACTIVITY
	ADVANCED RESEARCH PROJECTS AGENCY NUCLEAR TEST DETECTION OFFICE WASHINGTON, D. C.

13 ABSTRACT

This report discusses the work performed by SDL for the period January through March 1968, and is primarily concerned with seismic research activities leading to the detection and identification of nuclear explosions as distinguished from earthquake phenomenon. Also discussed are the data services performed for other participants in the VELA-UNIFORM project.

14. KEY WORDS

Seismic Data Laboratory - Quarterly
Technical Summary
VELA-UNIFORM Project

Unclassified
Security Classification